Resolving mid- to upper-crustal exhumation through apatite petrochronology and thermochronology

Gilby Jepson, Barbara Carrapa, Sarah W.M. George, Antoine Triantafyllou, Shana Egan, Kurt Constenius, George Gehrels, Mihai Ducea

Version of Record: https://www.sciencedirect.com/science/article/pii/S0009254121000152
Manuscript_bfe12ad1cb1c4620c066469a7eea008c

Resolving mid- to upper-crustal exhumation through apatite petrochronology and thermochronology

Gilby Jepson[*1], Barbara Carrapa[1], Sarah W. M. George[1], Antoine Triantafyllou[1, 2, 3], Shana M. Egan[1], Kurt N. Constenius[1], George E. Gehrels[1], and Mihai N. Ducea[1, 4]

[1] *Department of Geosciences, University of Arizona, Tucson, Arizona, USA*

[2] *Department of Geology, University of Liège, 4000 Sart Tilman, Belgium*

[4] *Faculty of Geology and Geophysics, University of Bucharest, Bucharest, Romania.*

[3] *Laboratoire de Géologie de Lyon : Terre, Planètes, Environnement, Université de Lyon, France*

November 25, 2020

Abstract

Double-dating using the apatite U-Pb and fission-track systems is becoming an increasingly popular method for resolving mid- to upper- crustal cooling. However, these thermochronometers constrain dates that are often difficult to link through geological time due to the large difference in temperature window between the two systems (typically >250°C) . In this study, we apply apatite U-Pb, fission-track, and apatite and whole rock geochemistry to fourteen samples from four tectonic domains common in Cordilleran orogenic systems: (1) basement cored-uplifts, (2) plutons intruded through a thick crustal column, (3) metamorphic core complexes and associated detachment faults, and (4) rapid, extrusive volcanic cooling, in order to provide a link between *in situ* geochemical signatures and cooling mechanisms. Comparisons of trace element partitioning between apatite and whole rock geochemistry provide insights into initial apatite-forming processes and/or subsequent modification. Apatite trace element geochemistry and the Th/U and La/Lu_N ratios provide tools to determine if an apatite is primary and representative of its parent melt or if it has undergone geochemical perturbation(s) after crystallization. Further, we demonstrate that by using a combined apatite U-Pb, FT, trace element, and whole rock geochemistry approach it is possible to determine if a rock has undergone monotonic cooling since crystallization, protracted residence in the middle crust, and provide unique structural

*corresponding author (gjepson@arizona.edu)

information such as the history of detachment faulting. Insights provided herein offer new applications for apatite thermochronology.

1 Introduction

Due to the low-solubility of phosphorous in silicate-rich melts and its incompatible behavior with many major rock-forming mineral phases, apatite is a common accessory mineral found in a wide range of crustal rocks (Chew & Spikings 2015). Apatite occurs as an accessory phase in many igneous and metamorphic rocks, and can be abundant in clastic sedimentary rocks (e.g., Henrichs et al. 2018, O'Sullivan et al. 2020, Chew et al. 2020). As well as being a readily available mineral phase, apatite incorporates trace amounts of radiogenic elements such as ^{238}U, ^{235}U, and ^{232}Th, making it a useful geo- and thermo- chronometer (Carrapa et al. 2009, Cherniak et al. 1991). Apatite is used as a low-temperature thermochronometer through fission-track and (U-Th-Sm)/He) thermochronometric techniques, which constrains the thermal evolution of a sample through the upper crust thus providing insights in to erosional and tectonic processes (e.g., Fitzgerald et al. 1993, Ehlers 2005, Reiners & Brandon 2006, Braun et al. 2006)

Improvement in Laser Ablation-Inductively Coupled Plasma-Mass Spectrometry (LA-ICP-MS) instrumentation and standards have facilitated progress in the development and application of apatite uranium-lead thermochronology (AUPb, e.g., Carrapa et al. 2009, Thomson et al. 2012, Chew et al. 2014). The apatite U-Pb system is controlled by the thermally activated volume diffusion of radiogenic lead at temperatures between (~375 and 570°C; e.g., Cochrane et al. 2014), thus, AUPb acts as a medium-temperature thermochronometer (e.g., Cherniak et al. 1991, Watson & Cherniak 2013). However, apatite is also susceptible to recrystallization, emphasizing the need for thorough interpretation of apatite U-Pb ages (e.g., Spear & Pyle 2002, Kusebauch et al. 2015, Odlum & Stockli 2020). The ~375-570°C temperature window is valuable as it provides information on the cooling history of a rock through the middle crust making the apatite U-Pb system a useful chronometer to a variety of geological questions such as tectonic exhumation (e.g., Odlum & Stockli 2019, 2020), ore formation (e.g., Belousova et al. 2002*a*, Glorie et al. 2019), and metamorphism (e.g., Schneider et al. 2015). Through the application of LA-ICP-MS, U-Pb and FT/(U-Th-Sm)/He (~60-120°C and ~80-45°C, respectively) apatite thermochronology can be integrated together in the form of double and triple-dating of a single mineral to constrain a rocks middle to upper crustal evolution (e.g., Jepson et al. 2018, Horne et al. 2019). Despite the use of the single-grain double and triple-dating method, it remains difficult to connect the ~500-60°C thermal and crustal history

of a rock in complex tectonic settings due to substantial ambiguities in thermal pathways (i.e. monotonic cooling *versus* more complex pathways such as reheating, Figure 1).

In addition to U-Pb dating, *in situ* trace and rare earth elements (REE) concentrations can also be analyzed simultaneously on high resolution single collector ICP-MS. While similar to procedures have been applied to zircons (Belousova et al. 2002*b*, Grimes et al. 2015, Chapman et al. 2016, Balica et al. 2020), . Trace elements in apatite are far more diagnostic of their host rock and a faithful recorder of the parent melt geochemistry (e.g. Prowatke & Klemme 2006, Jennings et al. 2011, Mark et al. 2016, O'Sullivan et al. 2018, Gillespie et . In particular, trace elements can be used in conjunction with apatite U-Pb thermochronology to understand magma formation and storage (Nathwani et al. 2020) and have even been shown to preserve complex diffusion profiles, demonstrating the application of apatite as a novel middle-crust petrochronometer (Seymour et al. 2016, Smye et al. 2018). The variety in radiometric dating and geochemical applications suggests that apatite can not only provide information on timing of cooling, but shed light on the mechanisms driving cooling and on the original whole rock chemistry (e.g., Bruand et al. 2016, 2017, O'Sullivan et al. 2020).

Here, we apply U-Pb, FT, and trace element analyses to single apatite grains, along with whole rock geochemistry to samples taken from different tectonic domains within the North American Cordillera: (1) cratonic-basement from Laramide basement cored-uplifts (Stevens et al. 2016); (2) Laramide-aged plutons related to a thickened crust (DeCelles 2004); (3) metamorphic core complex (MCC) and associated detachment faults (Lister & Davis 1989), and (4) syn- to post- core-complex extrusive volcanism (Best et al. 2009); with the aim of exploring the relationships between apatite U-Pb, apatite fission-track thermochronology and their trace element signatures as related to different tectonic processes (Figure 1 and 2).

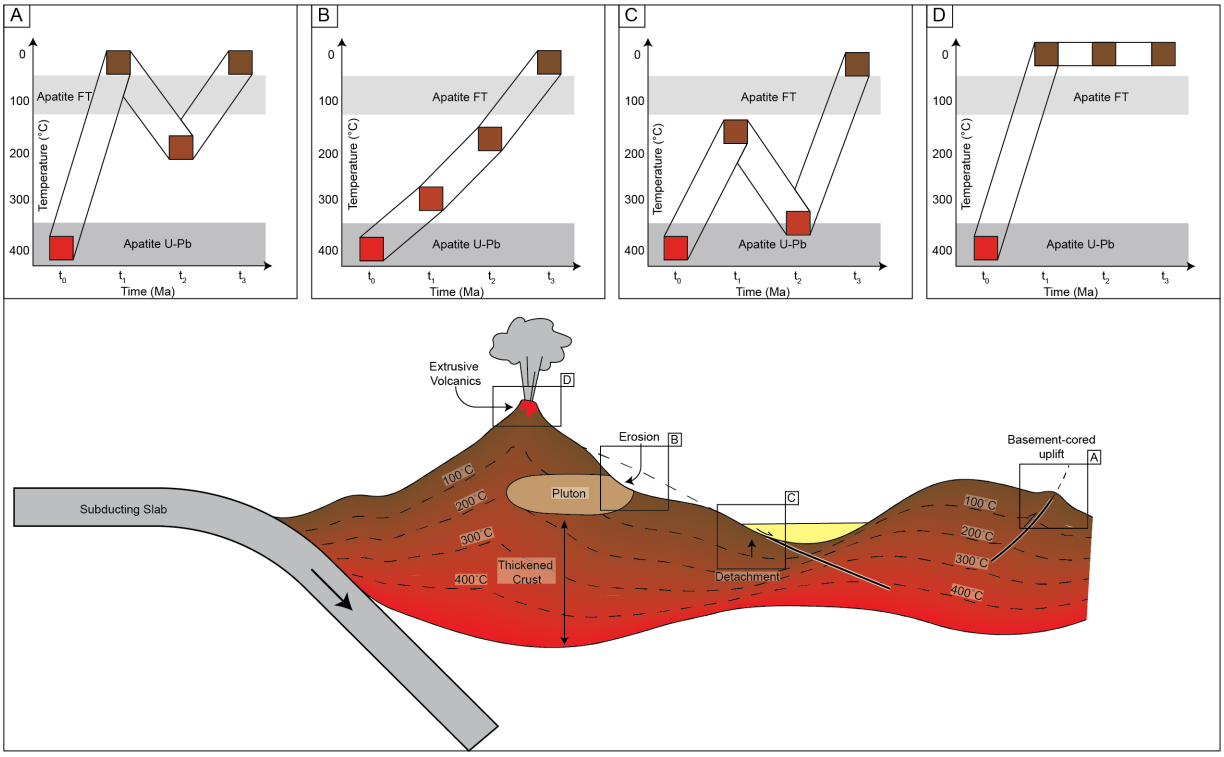

Figure 1: Schematic cross-section illustrating typical tectonic processes in a Cordilleran type margin and commonly associated thermal histories associated with each tectonic process. A) prolonged emplacement at mid-to-low temperatures in the shallow crust along basement-cored uplifts, B) steady monotonic cooling from mid-to-low temperatures via erosion of an intrusive pluton that has formed in thickened crust, C) multiple phases of mid-temperature reheating and cooling associated with tectonic exhumation along detachment faults, and D) extrusive volcanic rocks preserving rapid monotonic cooling.

2 Tectonic setting of the North American Cordillera

The North American Cordillera extends from Alaska in the north down to Mexico in the south and is part of the Circum-Pacific orogenic belt (e.g., DeCelles 2004, DeCelles et al. 2009). The North American Cordillera formed largely in response to continuous Late Paleozoic to Cenozoic subduction deforming thick passive margin strata atop cratonic basement (e.g., Coney et al. 1980, Dickinson 2004, Lawton 2008, Yonkee & Weil 2

The well-documented tectonic record of deformation, thickening, magmatism, and extensional collapse preserved along the North American Cordillera (e.g. Price 1986, Coney 1987, Wernicke et al. 1987, Sonder & Jones 19 make it and ideal setting for fingerprinting cooling and geochemical changes characteristic of different tectonic settings.

2.1 Archean Craton

The Wyoming craton is a segment of Archean crust which preserves predominately rocks of *ca.* 3.5-2.6 Ga and up to *ca.* 4.0 Ga(Hoffman 1988, Frost et al. 1998, Mueller & Frost 2006). The Wyoming craton collided with Laurentia in the Paleoproterozoic during the Trans-Hudson Orogeny to form the core of the North American continent (e.g., Mueller & Frost 2006, Whitmeyer & Karlstrom 2007). The western margin of Laurentia experienced Neoproterozoic and Paleozoic passive margin sedimentation prior to disruption by the Antler orogeny during the Late Devonian-Mississippian and the Sonoman orogeny in the Triassic (e.g., Burchfiel et al. 1992, Dickinson 2004, Gehrels & Pecha 2014). Following mid-Paleozoic orogenesis the western Laurentian margin underwent a mix of Triassic continental and marine sedimentation and Lower to Middle Jurassic terrane accretion consolidating the North American margin by the Late Jurassic (Dickinson & Lawton 2001, DeCelles 2004).

2.2 North American Cordilleran deformation and crustal thickening

The onset of Farallon plate subduction along the western margin of North America occurred during the Late Jurassic (e.g., Burchfiel et al. 1992, Dickinson 2004, DeCelles 2004). Oblique, east-dipping subduction increased from 5 cm/yr in the Jurassic to ~10 cm/yr in the Cretaceous (SW-NE, e.g., Engebretson et al. 1985, Weil & Yonkee 2012). The rapidly converging Farallon plate generated the Sevier fold-thrust belt, a region of thin-skinned deformation in the western North American Paleozoic-early Mesozoic sedimentary sequences (e.g., DeCelles 2004, Weil & Yonkee 2012, Yonkee & Weil 2015, Saylor et al. 2020, Figure 2). In the late Cretaceous, the Farallon slab shallowed resulting in flat slab subduction from California inboard (e.g., Coney & Reynolds 1977, Henderson et al. 1984, Bird 1998, Saleeby 2003, Humphreys 2009, Liu et al. 2010, Be Slab flattening has been variably attributed to interactions with the cratonic lithospheric keel or shallowing due to subduction of a Shatsky Rise conjugate (Liu et al. 2010, Jones et al. 2011, Carrapa et al. 2019). Regardless of the precise mechanism, flat-slab subduction during the late Cretaceous-early Paleogene caused deformation to propagate inboard, generating basement-involved uplifts known as the Laramide uplifts, which were exhumed and eroded during the late Cretaceous and early Cenozoic (e.g., Dickinson & Snyder 1978, Schmidt & Garihan 1978, Brown 1988, Erslev 1993, Peyton et al. 2012, Carrapa et a In addition to the Laramide orogeny, flat slab subduction significantly thickened the North American crust leading to regionally widespread metamorphism and magmatism (e.g., Terrien 2012, Fornash et al. 2013, Whitney et al. 2013, Behr & Smith 2016). Thus, the Wyoming craton remained at shallow crustal depths prior to being exposed via reverse faults, whereas the precondition for for tectonic exhumation

of metamorphic core complexes was thick-crust and extensive mid-crustal magmatism and associated metamorphism.

2.3 Slab rollback and magmatism

Foundering and subsequent rollback of the Farallon slab initiated in the late Paleogene (Bird 1979, Constenius 1996, Smith et al. 2014, Cassel et al. 2018). Removal of the flat slab and the change from subduction to transform plate boundaries between the Pacific and North American plate caused crustal collapse of the thickened North American crust and induced regional-scale extension across North America exhuming Metamorphic Core Complexes (MCC) along large-wavelength detachment faults (e.g., Atwater 1970, Davis 1980, Dewey 1988, Lister & Davis 1989, Spencer & Reynolds 1990, Spencer et al. 2019). The thickened crust and elevated geothermal gradient in the lower to middle crust during the Laramide orogeny set the precondition for "flareup" magmatism, characterized by extensive extrusive silicic magmatism that is suggested to have swept westward from the Eocene to Miocene (*ca.* 49-18 Ma) tracking the rollback of the Farallon slab and associated asthenosphere mantle upwelling (e.g., Coney 1978, Constenius et al. 2003, Best et al. 2016).

3 Materials and methods

3.1 Sample sites

Five samples (KC82317-1, KC82317-3, KC82816-1, KC82816-2 and KC82816-3) were collected from Archean to Paleoproterozoic rocks exposed along basement-cored uplifts in southwestern Montana (Table 1 and Figure 2, Carrapa et al. 2019). Zircon U-Pb dating on exposed Archean and Paleoproterozoic crystalline basement constrain ages ranging from 2.5-1.6 Ga with a prominent distribution at *ca.* 1.7-1.8 Ga (Foster et al. 2006).

Two samples (KJJ09-7 and KJJ09-8) were collected from Laramide-aged plutons exposed in the Santa Catalina mountains, Arizona (Table 1 and Figure 2). Samples KJJ09-7 and KJJ09-8 were identified as Laramide intrusive rocks with Cretaceous zircon U-Pb ages of 69.1 and 73.0 Ma, respectively (Fornash et al. 2013).

Three samples (MG1655, MG2465 and MG3150) were collected along a transect in the Pinaleño Mountain core complex, Arizona (Table 1 and Figure 2). Samples MG2465 and MG3150 were collected from an orthogneiss and a granodiorite, respectively, comprising the Proterozoic metamorphic core (Long

et al. 1995, Johnson & Arca 2010). Sample MG1655 was collected from a Proterozoic-mapped granite which hosts a strong mylonitized fabric (Johnson & Arca 2010). In addition, sample KJJ09-3 is a sill of Laramide-age which hosts a mylonitic fabric related to the Catalina detachment fault and a Paleogene zircon U-Pb age of 56.6 Ma (Fornash et al. 2013).

Samples GM-03, GM-05 and GM-08 were collected from the Galiuro Mountain, Arizona (Table 1). The Galiuro Mountains contain a section of late Oligocene volcanic rocks typical of the large ignimbrite flare-up of the southwestern US (Best et al. 2009); with predominantly dacitic ignimbrites reaching up to 2 km thick in thickness and are dated by zircon U-Pb as 29-24 Ma (Creasey & Krieger 1978). These ignimbrites overlay a Precambrian basement section dominated by mid Proterozoic metasedimentary rocks intruded by 1.1 Ga mafic dikes of suspected hot spot origin (Dickinson 1991, Arca et al. 2010).

Table 1: Samples collected from the North American cratonic basement, Laramide-aged plutons, Metamorphic Core Complexes/Detachment faults, and Paleogene volcanic rocks: Age is the published age of the rock, Lat is the north latitude and Long is the west longitude using the WSM 84 coordination system, Elev is elevation in meters above sea level. Lithology notation; *MA* is Middle Archean, *LA* is Late Archean, *PP* is Paleoproterozoic, *K* is Cretaceous, and P_ϵ is Paleogene. AFT is apatite fission-track, AUPb is apatite uranium-lead and trace and rare earth elements, and WR is whole rock geochemistry.

Sample	Formation	Region	Lithology	Age	Lat	Long	Elev	Method
Basement-Cored Uplifts								
KC82317-1	Cratonic basement	Little Belt, Montana	Gneissic granite	PP	46.942	-110.745	1733	AFT/AUPb
KC82317-3	Intrusion	Little Belt, Montana	Diorite	PP	46.958	-110.754	1742	AFT/AUPb
KC82816-1	Cratonic basement	Gravelly Range, Montana	Schist	LA	44.885	-111.694	2350	AFT/AUPb
KC82816-2	Cratonic basement	Gravelly Range, Montana	Gneiss	MA	44.888	-111.643	2120	AFT/AUPb
KC82816-3	Cratonic basement	Gravelly Range, Montana	Granite/ Gneiss	PP	45.318	-111.846	1929	AFT/AUPb
Thickened Crust/Laramide Plutons								
KJJ09-7	Leatherwood Intrusion	Santa Catalina, Arizona	Granodiorite	K	32.452	-110.752	2337	AFT/AUPb/ WR
KJJ09-8	Rice Creek Porphyry	Santa Catalina, Arizona	Hypabyssal granite	K	32.479	-110.697	1424	AFT/AUPb
Metamorphic Core Complex/Detachment Fault								

MG1655	Core Complex Granite	Pinaleño Mts, Arizona	Mylonitized Granite	PP	32.745	-109.840	1655	AFT/AUPb/ WR
MG2465	Core Complex Granite	Pinaleño Mts, Arizona	Foliated Granite	PP	32.717	-109.855	2465	AFT/AUPb/ WR
MG3150	Core Complex Gneisses	Pinaleño Mts, Arizona	Granodiorite	PP	32.692	-109.864	3150	AFT/AUPb/ WR
KJJ09-3	Catnip Sill	Santa Catalina, Arizona	Peraluminous granite	P_ϵ	32.354	-110.723	1608	AFT/AUPb/ WR
Extrusive Volcanic Rocks								
GM-03	Galiuro Volcanics	Galiuro Mts, Arizona	Welded Tuff	P_ϵ	32.657	-110.357	1534	AFT/AUPb/ WR
GM-05	Galiuro Volcanics	Galiuro Mts, Arizona	Welded Tuff	P_ϵ	32.658	-110.316	1885	AFT/AUPb/ WR
GM-05	Galiuro Volcanics	Galiuro Mts, Arizona	Welded Tuff	P_ϵ	32.688	-110.441	1620	AFT/AUPb/ WR

153

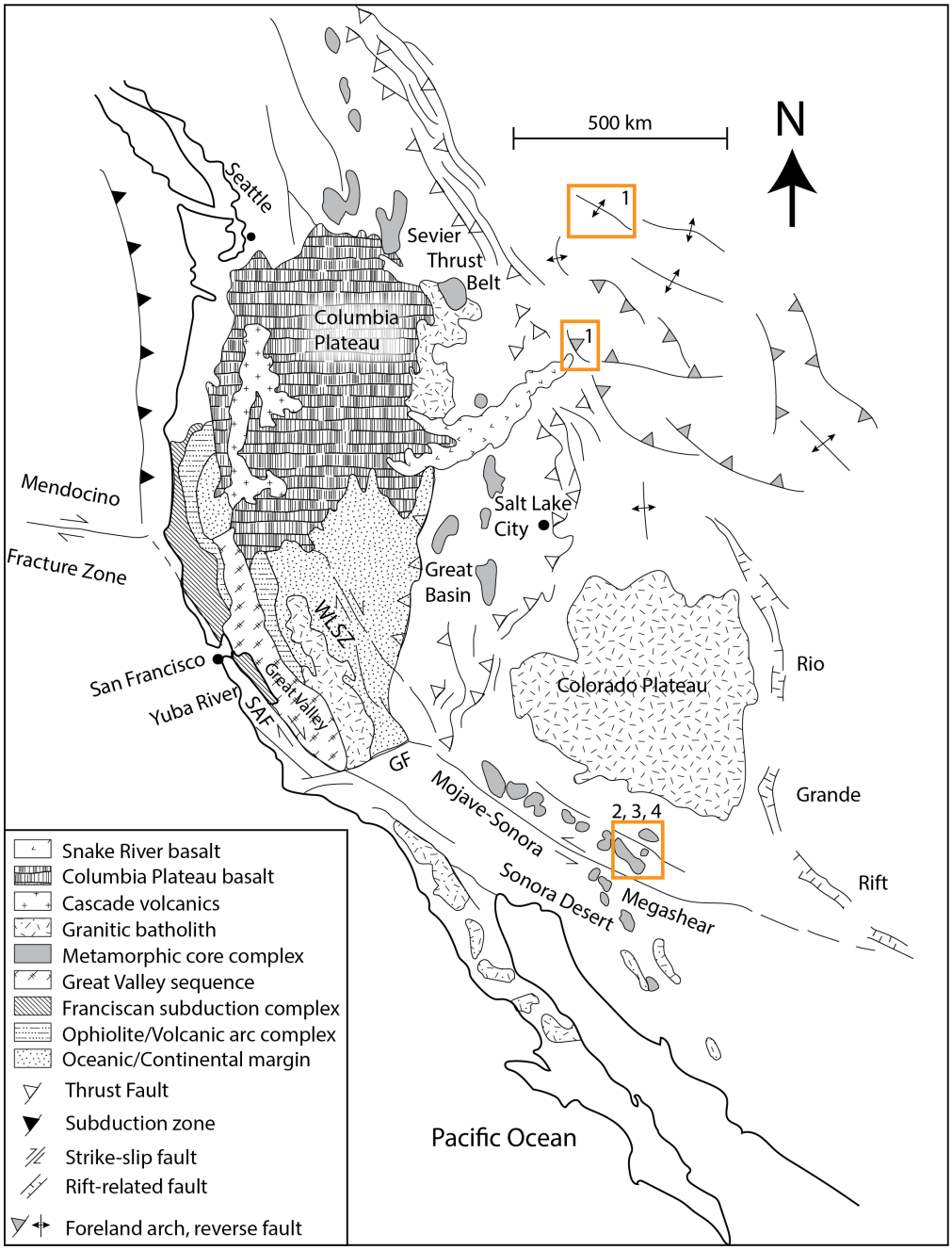

Figure 2: A schematic map of the western US Cordillera illustrating the key tectonic and magmatic processes: 1) Basement cored uplifts, 2) emplacement of Laramide-related plutons, 3) formation of metamorphic core complex and associated detachment faults, and 4) emplacement of Paleogene extrusive volcanic rocks. Map modified from Dilek & Moores (1999).

3.2 Apatite fission-track thermochronology

Apatite fission-track (AFT) analyses were performed using the external detector method (Tagami 1987). Apatite grains were mounted in epoxy and polished, and spontaneous fission tracks were revealed by etching with 5.5-M nitric acid for 20 s at 21°C before irradiation (after Donelick et al. 2005). The

neutron fluence was monitored using CN5 U-doped glass (Bellemans et al., 1995). The irradiation was performed at Oregon State University. After irradiation, mica external detectors were etched in 40% hydrofluoric acid for 45 min at 21°C (after Donelick et al. 2005). Analyses were conducted for optical identification of fission-tracks using an Olympus microscope at 1600X magnification with a drawing tube located above a digitizing tablet and a Kinetek computer-controlled stage driven by the FT Stage program provided by Trevor Dumitru of Stanford University. The fission-track analyses were performed at the Arizona Fission Track Laboratory in the University of Arizona (Table 3 and 4, and Supplementary Table 2). Confined tracks were measured to provide information on the time spent in the 120-60°C apatite partial annealing zone (APAZ), with longer mean confined track lengths (>13.5μm) defining rapid cooling through the APAZ and shorter mean confined track lengths indicating prolonged residence in the APAZ (e.g., Laslett et al. 1982, Gleadow et al. 1986, Donelick & Miller 1991, Tagami & O'Sullivan 2005).

Samples KC82317-1, KC82317-3, KC82816-1, KC82816-2 and KC82816-3 were selected for apatite U-Pb and FT single-grain double dating. The concentration of uranium (^{238}U) in the counted areas of apatite was determined using LA-ICP-MS. Age calculation was carried out using in-house R script following equations as described in Hasebe et al. (2004) and Vermeesch (2017), using the Durango apatite (McDowell et al. 2005) to perform a session-zeta calibration (Vermeesch 2017). For details on trace element acquisition, see section 3.4.

3.3 Apatite U-Pb thermochronology

The AUPb method relies on the thermally activated volume diffusion of Pb within the crystal lattice of an apatite grain to provide information about its thermal history cochrane2014high, seymour2016tectonics, glorie2017ther Estimates of the closure temperature of the AUPb system are between *ca.* 550 and 370°C depending on cooling rates and apatite crystal sizes (Chew & Donelick 2012, Thomson et al. 2012, Cochrane et al. 2014, Gillespie et al. 2018), although temperatures of *ca.* 450-550°C are more typically reported (e.g., Schoene & Bowring 2007, Blackburn et al. 2011). Apatite grains that were selected for AFT analysis were also targeted for same-grain AUPb and *in situ* trace element analyses. The AUPb dates for this study were acquired using a Photon Machine Analyte G2 Excimer 193 nm laser ablation system connected to a Thermo Element2 single-collector High Resolution ICP-MS at the Arizona LaserChron Center. Spot ablations were performed using a 30 μm spot size and a 5 Hz laser repetition rate. Each analysis comprised 20s background collection (laser off) and 40.2 s apatite ablation (laser on; see detailed operational conditions in Table 2). During apatite U-Pb analysis, the Madagascar (MAD2) apatite primary reference

material (reference age 474.2±0.4 Ma, Thomson et al. 2012) was measured repeatedly throughout the session to correct for instrumental drift and down hole fractionation, and the Mt. McClure (523.98 ± 0.12 Ma Schoene & Bowring 2006) reference material was analyzed as a secondary standard for accuracy checks (Mt. McClure = 514.6 ± 2.0 Ma, Supplementary File 5). Data reduction was performed using the "*VizualAge_UcomPbine*" Data Reduction Scheme (DRS) in Iolite (Paton et al. 2011, Chew et al. 2014). More details on this DRS can be found in Chew et al. (2014). Isotopic data (238/206 and 207/206 ratios) were plotted and apatite U-Pb ages were obtained using a Tera-Wasserburg lower concordia intercept based on a unique upper ($^{207}Pb/^{206}Pb$) of a relevant non-radiogenic Pb regression line Figures 3-6. Tera-Wasserburg plots were calculated using the IsoplotR package v.2.3 (Vermeesch 2018) in R v.3.5.2.

3.4 Apatite trace element analysis

A range of trace elements were measured simultaneously to the acquisition of U and Pb isotopes through LA-ICPMS (Table 2 Supplementary File 4, Chapman et al. (2016)). These elements were selected based on their potential to inform on source rock processes (e.g. Belousova et al. 2002*b*, Chapman et al. 2016, Bruand et al. 2017, Henrichs et al. 2018, Gillespie et al. 2018). Trace element data reduction were performed using the 'X_Trace_Elements_IS' DRS in Iolite (Paton et al. 2011) following Chew et al. (2016). Instrumental drift was corrected using NIST610 as the primary standard and elemental concentrations were calculated using ^{43}Ca for internal standardization using stoichiometric abundance of Ca at 39.74 wt% (Chew et al. 2014). Individual element concentrations for standards NIST610 glass, MAD2 apatite, Durango apatite, and McClure Mountain apatite can be found in Supplementary File 3.

Table 2: Analytical parameters for apatite U-Pb and trace and rare earth element (REE) analyses using Laser Ablation Inductively Coupled Plasma Mass Spectrometry (LA-ICP-MS). MFC is mass flow controller for He gas. Acquisition time and settling time are listed in order of isotopes measured. For a detailed list of LA-ICP-MS parameters, see Supplementary File 4.

Parameters	**Apatite U-Pb and trace and REE**
Laser Parameters	
Instrument	Photon Machines Analyte G2 excimer laser 193 nm
Washout	20s
Background	9s
Analysis Duration	40.2s
Laser Repetition	5 Hz
Spot Size	30μm
Energy	3.9 J/cm^2
MFC1, MFC2 (L/min)	0.11, 0.29
Mass Spectrometer	
Instrument	Thermo Element 2
Number of Isotopes measured	^{29}Si, ^{35}Cl, ^{43}Ca, ^{51}V, ^{55}Mn, ^{88}Sr, ^{89}Y, ^{91}Zr, ^{139}La, ^{140}Ce, ^{141}Pr, ^{146}Nd, ^{147}Sm, ^{153}Eu, ^{157}Gd, ^{159}Tb, ^{163}Dy, ^{165}Ho, ^{166}Er, ^{169}Tm, ^{172}Yb, ^{175}Lu, ^{202}Hg, ^{204}Pb, ^{206}Pb, ^{207}Pb, ^{208}Pb, ^{232}Th, ^{238}U

3.5 Whole rock geochemistry

Samples were cut and finely molded in agate jars. Approximately 50 mg of each rock powder was dissolved by two successive acid attacks. Samples were firstly dissolved in a HF:HNO_3 concentrate mixture (2:1) in 6 mL Savillex® standard octagonal bodied PFA Teflon vials. These Teflon vials, generally referred as Teflon bombs, were sealed using a wrench top closure and Ultem® socket cap. Teflon vials were then set into an oven at 130°C for 5 days (see similar approach described in Inglis et al. 2018). Solutions were then evaporated on hot plates, and residues were re-dissolved in a HCl concentrate (16M) solution and put on hot plate (120°C) for 24h. The solution was then re-evaporated, and residue dissolved in 2% nitric acid for chemical analysis. Samples were centrifuged to remove undissolved material from the solution. Samples run for trace element analysis were diluted to 10 mL with 2% nitric acid. Trace element analyses were conducted in solution on a ThermoFisher X-Series II Quadrupole Inductively Coupled Plasma Mass Spectrometer (Q-ICP-MS) at the Geosciences Department at the University of Arizona, following the procedures outlined in Rossel et al. (2013). Trace element results were standardized to the Columbia River Basalt (BCR-2) USGS rock standard (Schudel et al. 2015). Standard error for samples run in solution is expected to be less than 5% for major elements and less than 3% for REEs. A blank composed of the same 2% nitric acid that was used to dilute the samples and standards was run before and after each

sample and standard to account for any material added by our matrix. Detailed whole rock geochemistry results can be found in Supplementary File 6.

4 Results

4.1 Basement-cored uplifts

4.1.1 Apatite U-Pb dating

All five samples from basement-cored uplifts clearly define linear arrays in Tera-Wasserburg concordia space (Figure 3A, D, G, J, and K). Using the lower intercept discordia, samples KC82317-1, KC82317-2, KC82816-2, and KC82816-3 yielded Paleoproterozoic ages of 1840 ± 14 Ma (MSWD = 0.42), 1858 ± 13 Ma (MSWD = 0.42), 1811 ± 31 Ma (MSWD = 8.0), and 1675 ± 17 Ma(MSWD = 0.7), respectively. Sample KC82816-1 yielded an Archean age of 2417 ± 32 Ma (MSWD = 3.3, Figure 3 and Supplementary Table 1).

4.1.2 Apatite fission-track thermochronology

Two samples (KC82317-1 and KC82317-3) from the Paleoproterozoic core of the Little Belt Laramide uplift in central Montana yielded Cretaceous AFT ages of 85 ± 4 Ma and 64 ± 3 Ma, respectively (Table 1 and Table 3). Confined fission-tracks from sample KC82317-3 provided a mean track length (MTL) of 14.2 ± 1.0 μm.

Three samples (KC82816-1, KC82816-2 and KC82816-3) from Archean and Paleoproterozoic rocks exposed along the Gravelly Range Laramide uplift in southwest Montana yielded Cretaceous AFT ages of 71 ± 7 Ma, 95 ± 12 Ma, and 74 ± 4 Ma, respectively (Table 1 and Table 3). Confined fission-tracks from samples KC82816-2 and KC82816-3 yielded relatively long MTLs of 14.2 ± 1.2 μm and 14.0 ± 0.9 μm, respectively.

Table 3: Summary of laser ablation apatite-fission track data from this: n = number of grains dated, N_s = number of spontaneous tracks counted, ρs = average spontaneous track density (x10^5cm^{-2}), ^{238}U = average uranium concentration of the analyzed grains, P(χ^2) = χ^2 probability after (Galbraith 1981), t is the central age (Ma), D_{par} = mean track etch pit diameter parallel to the crystallographic c-axis, P = pooled age, # is the number of confined tracks counted, MTL is the mean of measured confined tracks in μm and $\pm1\sigma$ is also in μm.

Sample	n	N_s	ρs	^{238}U (ppm)	P(χ^2)	t (Ma)	$\pm1\sigma$	D_{par} (μm)	P (Ma)	$\pm1\sigma$	#	MTL (μm)	$\pm1\sigma$

Basement-Cored Uplift													
KC82317-1	23	1183	16.4	44.2	0.17	64	3	2.2	52	8	-	-	-
KC82317-3	26	1391	27.7	59.9	0.15	85	4	2.5	85	14	50	14.2	1.0
KC82816-1	10	239	12.4	33.5	0.12	71	7	2.0	92	16	-	-	-
KC82816-2	11	148	5.0	10.2	0.06	95	12	2.2	129	24	28	14.2	1.2
KC82816-3	25	839	10.7	26.7	0.76	75	4	2.3	73	12	50	14.0	0.9

4.1.3 Apatite trace elements

Samples KC82317-1 and KC82317-3 both display REE patterns enriched in light REE (LREE) and depleted in heavy REE (HREE), as well as high mean values of La/Lu_N (N is for chondrite normalized) of 86.0 and 176.2 for KC82317-1 and KC82317-3, respectively (Figure 3. Sample KC82317-1 shows more variation in its LREE content (Figure 3 and 8); La/Sm_N ranging from 0.4 to 2.4 (median 1.3); as well as a distinctive negative Eu anomaly ($Eu/Eu^* = Eu_N/[Sm_N * Nd_N]^{1/2}$) ranging from 0.13 to 0.80 (median 0.27, compared to 0.78 for sample KC82317-3). Samples KC82816-1, KC82816-2, and KC82816-3 display various REE patterns (Figure 3). KC82816-1 shows a relatively flat REE pattern (La/Lu_N ranging from 0.9 to 18.2) with consistent concentrations of REE, 100 to more than 1000x chondritic values, along with a moderate negative Eu anomaly (Eu/Eu* from 0.49 to 0.63). Sample KC82816-2 shows convex-upward REE patterns (Figure 3), with depletion in L- and H-REE compared to Medium-REE (MREE; La/Sm_N: 0.05-0.35 and Dy/Yb_N: 2.21-3.94). Negative Eu anomaly ranging between 0.15 to 0.31 (median of 0.18). Sample KC82816-3 shows a similar pattern as KC82816-1 with a moderate Eu anomaly (Eu/Eu* median value: 0.48; Figure 3). However, it shows a pronounced depletion in HREE compared to MREE (Dy/Yb_N ranging from 1.20 to 2.97, median 1.54), similar to KC82816-2.

4.2 Laramide-aged plutons

4.2.1 Apatite U-Pb dating

Both samples from Laramide plutons clearly show linear arrays in Tera-Wasserburg concordia space (Figure 4A and D). Samples KJJ09-07 and KJJ09-08 yield lower intercept discordia ages of 40 ± 2 Ma (MSWD = 1.3), and 62 ± 21 Ma (MSWD = 2.3), respectively (Figure 4 and Supplementary Table 1).

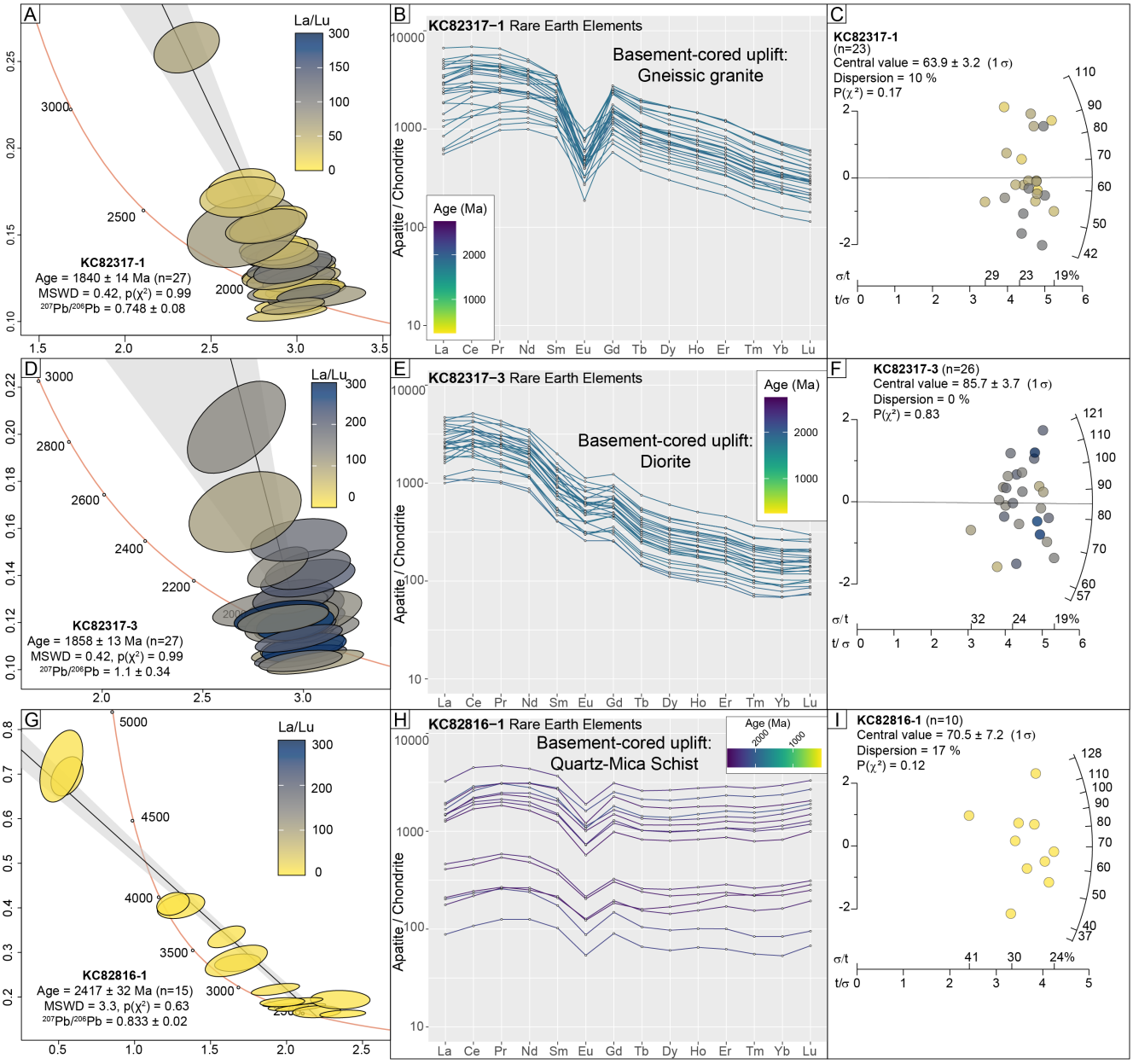

Figure 3: Tera-Wasserburg (T-W) concordia diagrams (A, D, G, J, and M), chondrite normalized REE profile plots (B, E, H, K, and N), and apatite fission-track radialplots (C, F, I, L, and O) for samples KC82317-1, KC82317-2, KC82816-1, KC82816-2, and KC82816-3. Apatite U-Pb analyses are plotted using IsoplotR (Vermeesch 2018) and colored according to their La/Lu_N ratio. On the T-W, Ellipses are plotted at 2σ, solid lines represent discordia projections used to obtain an estimate of the initial $^{207}Pb/^{206}Pb$ ratio. Chondrite values from Pourmand et al. (2012) and analyses are colored according to their ^{207}Pb corrected apatite U-Pb age based on the sample's unique discordia. Circles in the radial plots (Vermeesch 2009) are colored according to their La/Lu_N ratio, with blank circles representing grains that no geochemical data was obtained.

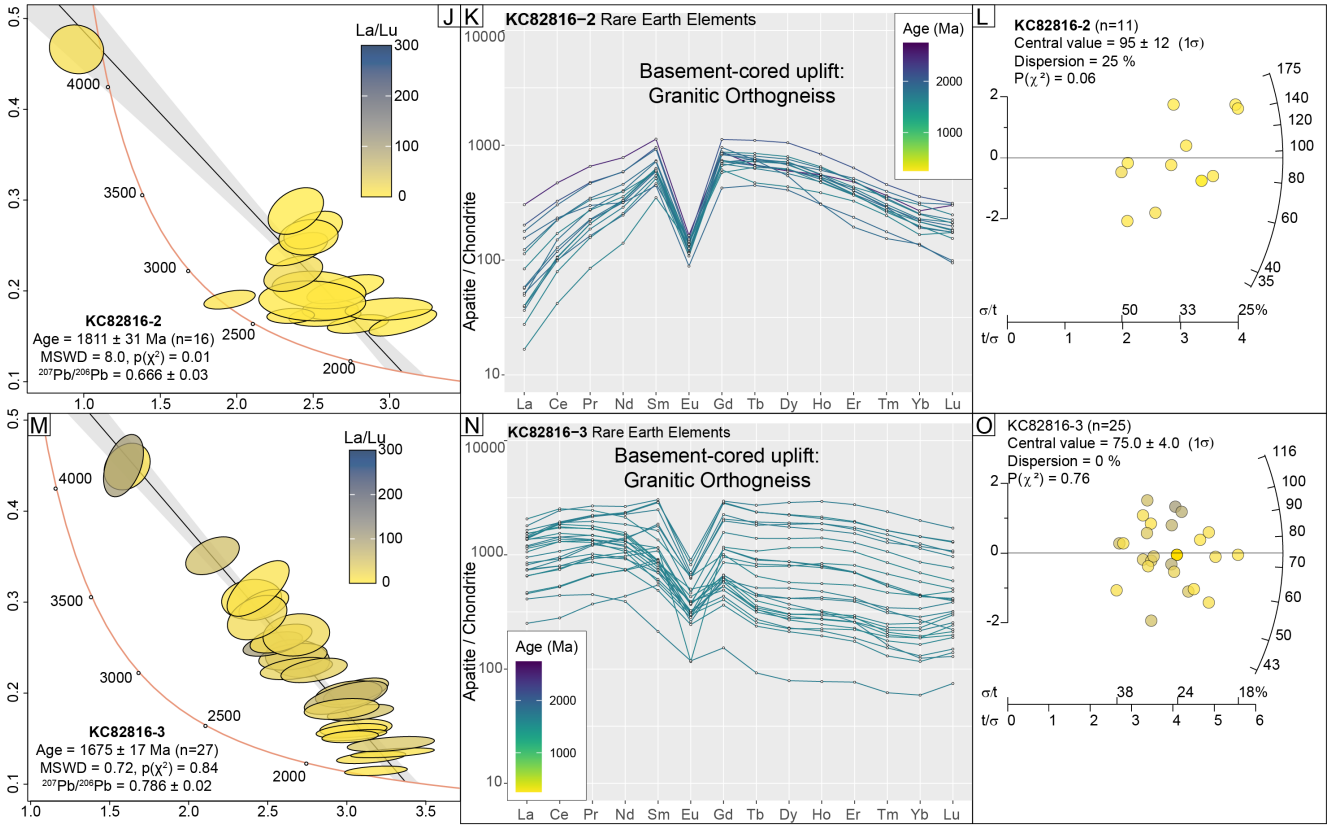

Figure 3: Continued.

4.2.2 Apatite fission-track thermochronology

Two samples (KJJ09-7, and KJJ09-8) from Laramide-aged plutons within the Santa Catalina Metamorphic Core Complex, Arizona yielded Paleogene-Neogene AFT ages of 24 ± 2 Ma and 41 ± 6 Ma, respectively (Table 1 and Table 4). Confined fission-tracks from sample KJJ09-07 yielded a long MTL of 13.7 ± 1.2 μm.

4.2.3 Apatite and whole rock trace elements

Samples KJJ09-07 and KJJ09-08 display similar REE patterns, with MREE content ~200x chondritic values. Apatites from both samples display positive LREE/HREE ratios (La/Lu_N ranging between 18.8-280.4 and 160.3-307.6, respectively) and moderately negative Eu anomaly (Eu/Eu* median values of 0.54 and 0.67, respectively). Whole rock REE for sample KJJ09-07 displays a REE profile enriched in LREE and depleted in HREE (La/Lu_N of 11.84) similar to *in situ* chemical analyses on constitutive apatites (Figure 3)

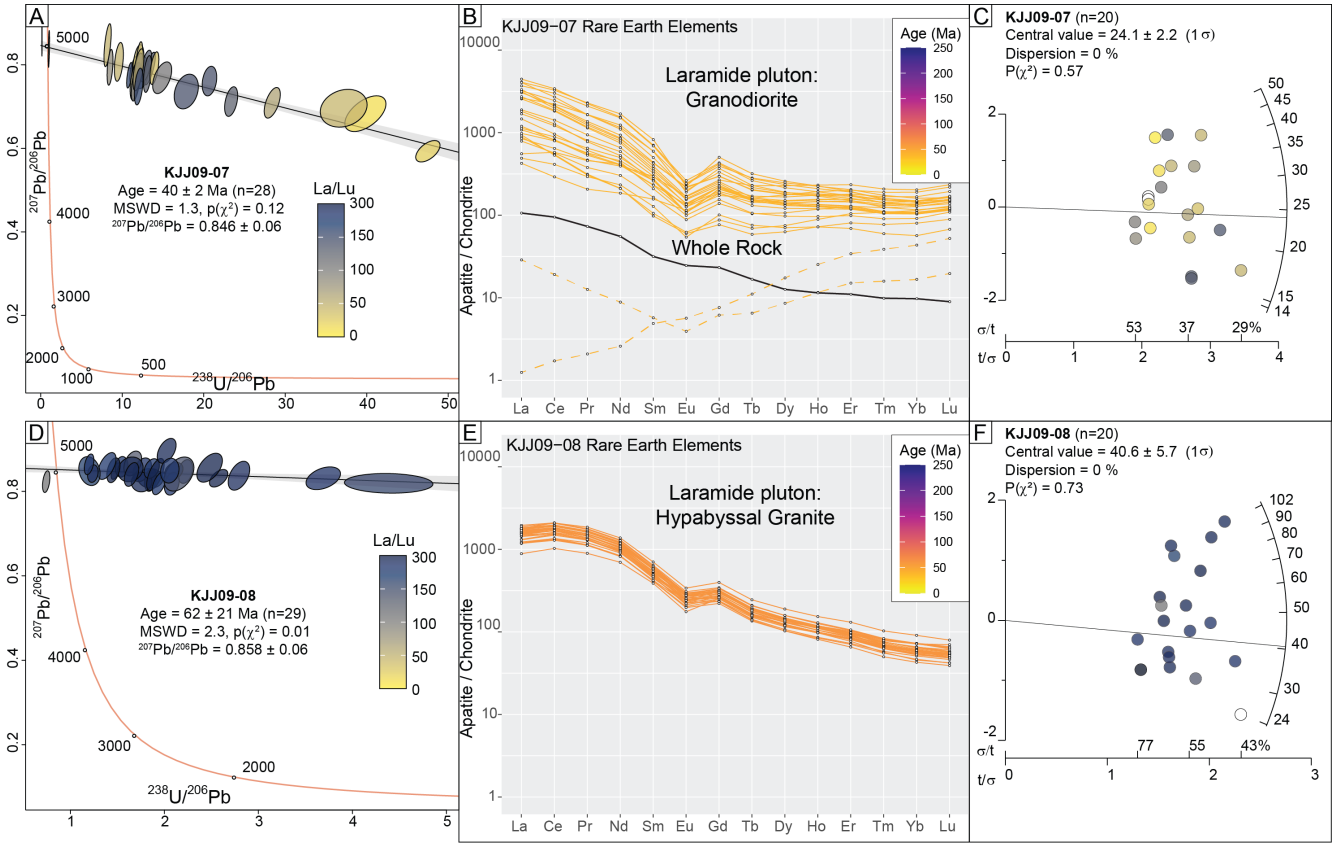

Figure 4: Tera-Wasserburg (T-W) concordia diagrams (A, D, and G), chondrite normalized REE spiderplots (B, E, and H), and apatite fission-track radialplots (C, F, and I) for samples KJJ09-03, KJJ09-07, and KJJ09-08. Apatite U-Pb analyses are plotted using IsoplotR (Vermeesch 2018) and colored according to their chondrite normalized La/Lu ratio. On the T-W, Ellipses are plotted at 2σ, solid lines represent discordia projections used to obtain an estimate of the initial $^{207}Pb/^{206}Pb$ ratio. Chondrite values from Pourmand et al. (2012) and analyses are colored according to their ^{207}Pb corrected apatite U-Pb age based on the sample's unique discordia. Solid black lines in the spiderplots are whole rock REE patterns. Circles in the radial plots (Vermeesch 2009) are colored according to their La/Lu_N ratio, with blank circles representing grains that no geochemical data was obtained.

4.3 Metamorphic Core Complex and detachment fault

4.3.1 Apatite U-Pb dating

Of the three MCC and detachment fault samples, two samples, MG3150 and MG2465 displayed scattered ellipses through Tera-Wasserburg concordia space (Figure 5A, D, and G). Sample MG3150 displays oscillatory zoning in cathodoluminescence (CL) images, whereas sample MG2465 preserves recrystallization textures (Supplementary File 8). Thus, we define two and one clear discordia arrays, respectively. Sample MG3150 yields a prominent Mesoproterozoic lower intercept discordia age (n = 17) of 1087 ± 13 Ma (MSWD = 2.0), with a secondary Devonian discordia age (n = 9) of 373 ± 18 Ma (MSWD = 3.9, Figure 5). Additionally, sample MG3150 preserves two ellipses that yield a *ca.* 700 Ma age, however two ellipses were deemed too few for a robust discordia age calculation (Supplementary Table 1). Sample MG2465 yields a prominent Neoproterozoic lower intercept discordia (n = 14) of 734 ± 23 Ma (MSWD = 1.6) with younger ellipses indicative subsequent of recrystallization. The two detachment faults MG1655 and KJJ09-03 both preserve homogeneous CL textures, a clear, linear array in Tera-Wasserburg concordia space and yield a lower intercept discordia ages of 22 ± 5 (MSWD = 0.5) and 39 ± 7 Ma (MSWD = 2.9), respectively (Figure 5G and J).

4.3.2 Apatite fission-track

Three samples (MG1655, MG2465, and MG3150) from Paleoproterozoic rocks exposed within the Pinaleño Mountain core complex, Arizona yielded Paleogene-Neogene AFT ages of 20 ± 2 Ma, 25 ± 3 Ma, and 29 ± 3 Ma, respectively (Table 1 and Table 4). Confined fission-tracks from samples GM3150 and MG2465 yielded MTLs of 13.8 ± 1.6 μm and 13.0 ± 1.7 μm, respectively. Sample KJJ09-3 from the detachment mylonitized granite along the Santa Catalina Metamorphic Core Complex, Arizona yielded Paleogene-Neogene AFT age of 21 ± 3 Ma (Table 4).

4.3.3 Apatite and whole rock trace elements

Sample MG3150 displays a variably fractionated REE profile (Figure 5), marked by minor to moderate LREE/HREE ratios (La/Lu_N ranging from 5.88 to 341.84, median of 94.84); and a minor depletion in Eu (Eu/Eu* median at 0.80). Fractionation of HREE compared to MREE is distinct in this sample (Dy/Yb_N range: 0.65-2.37). Sample MG2465 displays relatively flat REE patterns (in particular for HREE), with minor depletion in LREE (La/Sm_N ranging from 0.15 to 1.90, median of 1.12) and a noticeable depletion

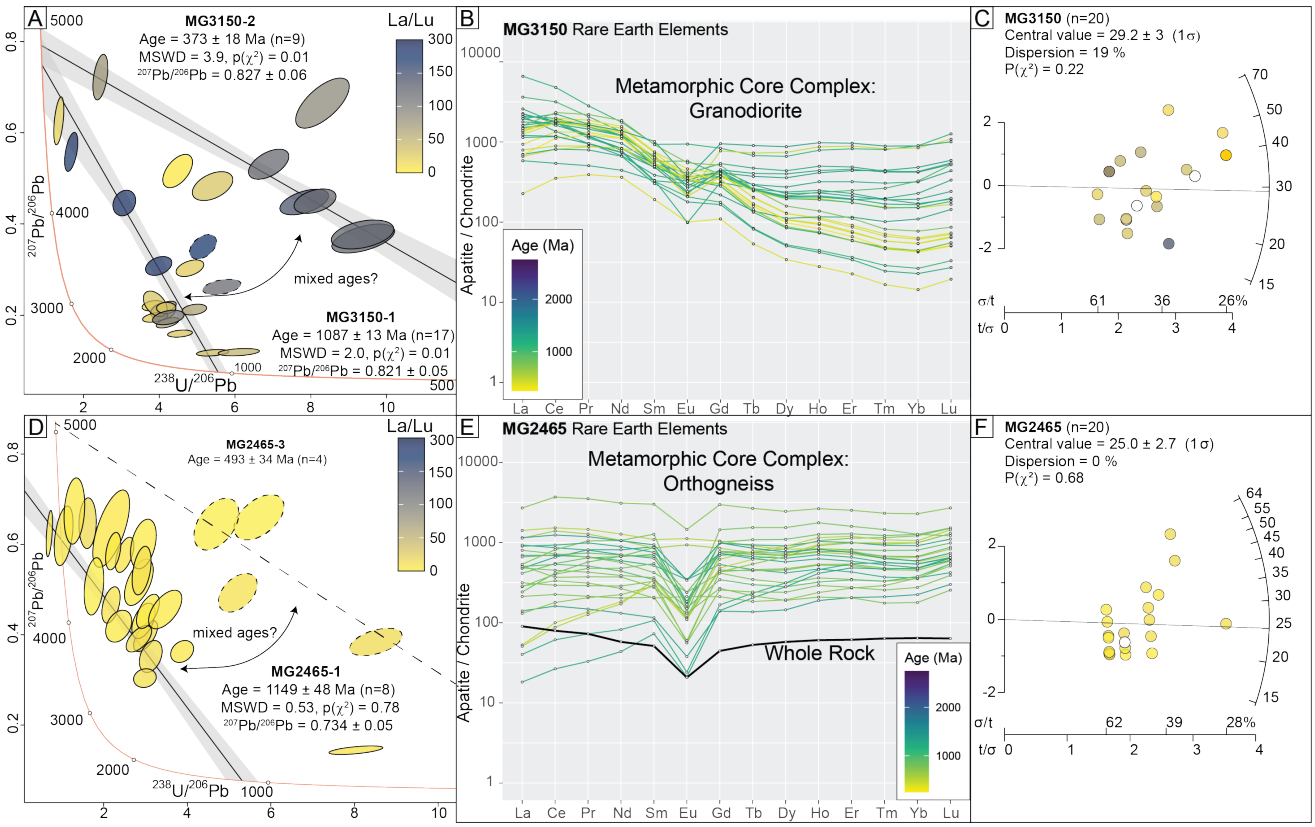

Figure 5: Tera-Wasserburg (T-W) concordia diagrams (A, D, G, and J), chondrite normalized REE spiderplots (B, E, H, and K), and apatite fission-track radialplots (C, F, I, and L) for samples MG3150, MG2465, MG1655, and KJJ09-03. Apatite U-Pb analyses are plotted using IsoplotR (Vermeesch 2018) and colored according to their La/Lu ratio. On the T-W, Ellipses are plotted at 2σ, solid lines represent discordia projections used to obtain an estimate of the initial $^{207}Pb/^{206}Pb$ ratio. Dashed lines represent a more uncertain discordia projection used to obtain an estimate of the initial $^{207}Pb/^{206}Pb$ ratio, dashed ellipses represent grains that were corrected using the more uncertain discordia. Chondrite values from Pourmand et al. (2012) and analyses are colored according to their ^{207}Pb corrected apatite U-Pb age based on the sample's unique discordia, mixed ages were calculated using an assumed initial $^{207}Pb/^{206}Pb$ ratio based on (Stacey & Kramers 1975). Solid black lines in the spiderplots are whole rock REE patterns. Circles in the radial plots (Vermeesch 2009) are colored according to their La/Lu_N ratio, with blank circles representing grains that no geochemical data was obtained.

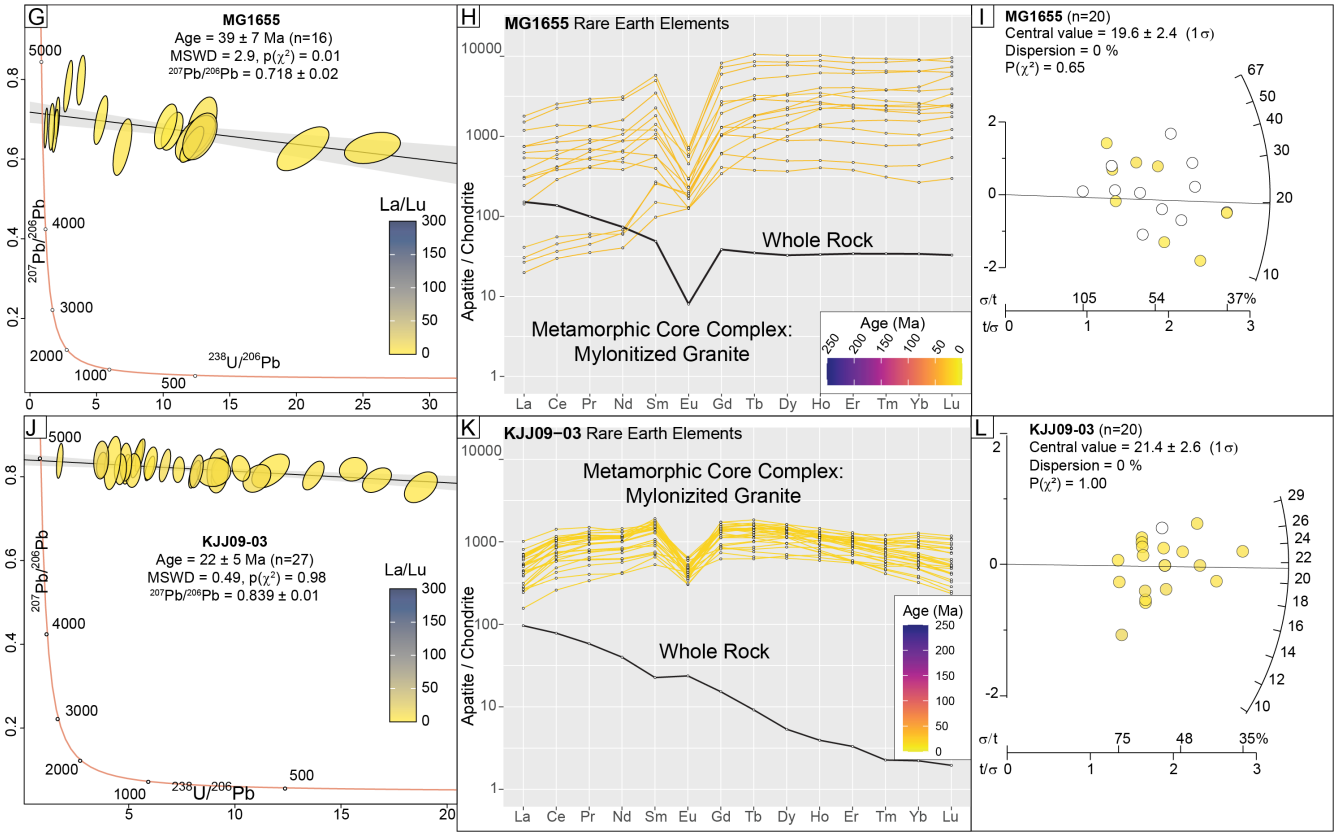

Figure 5: Continued.

in Eu (Eu/Eu* median value of 0.25). Whole rock REE composition for sample MG2465 mimics the REE pattern of constitutive apatites, with a flat trend and a distinctive Eu anomaly (Eu/Eu* of 0.43, Figure 5). In contrast, sample MG1655 shows variable fractionation trend of LREE in comparison to MREE (La/Sm_N from 0.10 to 1.35, median of 0.25) and relatively flat HREE distribution (Dy/Yb_N median value of 1.04; Figure 7). Eu anomaly is negative and moderate ranging from 0.10 to 0.69. In comparison, whole rock REE composition for sample MG1655 shows a similar trend (M- and HREE and Eu anomaly) except for LREE that appears enriched for the bulk rock composition (La/Sm_N of 3.11). All three samples display a large degree of variance between individual grain REE concentrations (Figure 5 and Figure 7).

Sample KJJ09-03 displays a flat to slightly convex-upward REE pattern (Figure 5K), with a moderate depletion in LREE (La/Sm_N range: 0.16-0.67) and in HREE (Dy/Yb_N range: 0.85-2.07, median of 2.04). Patterns are marked by a minor negative Eu anomaly (Eu/Eu* median at 0.36). In contrast, the whole rock REE composition for sample KJJ09-03 shows a high LREE/HREE ratio (La/Lu_N of 37.85) and no Eu anomaly (Eu/Eu* of 1.30).

4.4 Volcanic rocks

4.4.1 Apatite U-Pb dating

All three samples from the volcanic rocks clearly define linear arrays in Tera-Wasserburg concordia space (Figure 6A, D, and G). Samples GM-03, GM-05, and GM-08 yield Eo-Oligocene lower intercept discordia ages of 41 ± 12 Ma (MSWD = 1.6), 28 ± 31 Ma (MSWD = 1.2), and 29 ± 12 Ma(MSWD = 1.1), respectively (Figure 6 and Supplementary Table 1).

4.4.2 Apatite fission-track thermochronology

Three samples (GM-03, GM-05, and GM-08) from Paleogene volcanic rocks along the Galiuro Mountains in Arizona yielded AFT ages of 31 ± 4 Ma, 31 ± 6 Ma, and 29 ± 5 Ma, respectively (Table 1 and Table 4).

Table 4: Summary of external detector apatite fission track data from the North American Cordillera: n = number of grains dated, N_s = number of spontaneous tracks counted, ρs = average spontaneous track density (x10^5cm^{-2}), N_i = number of induced tracks counted, ρi = average induced track density (x10^5cm^{-2}), P(χ^2) = χ^2 probability after (Galbraith 1981), N_d = number of dosimeter tracks counted, ρi = average dosimeter track density (x10^5cm^{-2}), t is the central age (Ma), D_{par} = mean track etch pit diameter parallel to the crystallographic c-axis, # is the number of confined tracks counted, MTL is the mean of measured confined tracks in μm and $\pm1\sigma$ is also in μm. G. Jepson Zeta: 341.7 ± 8.

Sample	n	N_s	ρs	N_i	ρi	P(χ^2)	t (Ma)	$\pm1\sigma$	ρd	N_d	D_{par} (μm)	#	MTL (μm)	$\pm1\sigma$
Laramide Plutons														
KJJ 09-7	20	144	2.1	1249	18.1	0.50	24.1	2.24	12.3	5533	2.0	50	13.7	1.2
KJJ 09-8	20	79	1.1	364	5.2	0.66	40.6	5.66	12.1	5533	2.0	-	-	-
Metamorphic Core Complex														
MG1655	20	78	1.5	939	18.3	0.54	19.6	2.38	13.8	5533	2.1	-	-	-
MG2465	20	106	1.4	970	13.0	0.60	25.0	2.65	13.4	5533	2.4	14	13.0	1.7
MG3150	20	156	3.0	1193	23.2	0.25	29.2	2.97	13.0	5533	2.0	38	13.8	1.6
KJJ 09-3	20	80	1.0	770	10.0	0.47	21.4	2.58	12.1	5533	2.0	-	-	-
Extrusive Volcanic Rocks														
GM-03	20	77	1.2	697	11.2	0.84	30.8	3.8	16.4	5533	2.2	-	-	-
GM-05	20	32	1.0	287	8.9	0.96	30.5	5.7	16.0	5533	2.4	-	-	-
GM-08	20	38	1.0	345	9.4	0.92	28.6	5.0	15.2	5533	2.2	-	-	-

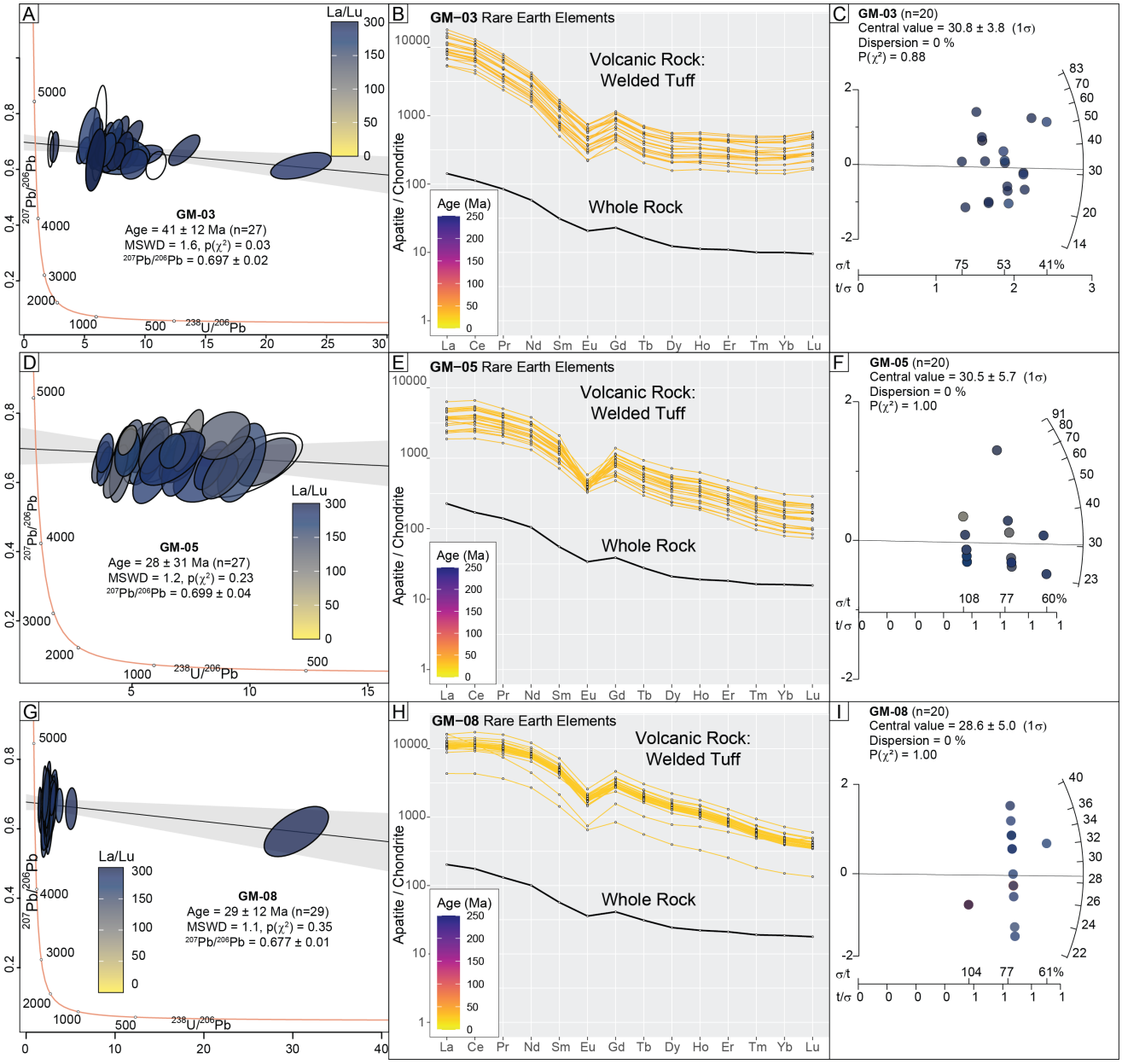

Figure 6: Tera-Wasserburg (T-W) concordia diagrams (A, D, and G), chondrite normalized REE spiderplots (B, E, and H), and apatite fission-track radialplots (C, F, and I) for samples GM-03, GM-05, and GM-08. Apatite U-Pb analyses are plotted using IsoplotR (Vermeesch 2018) and colored according to their La/Lu ratio. On the T-W, ellipses are plotted at 2σ, solid lines represent discordia projections used to obtain an estimate of the initial $^{207}Pb/^{206}Pb$ ratio. Chondrite values from Pourmand et al. (2012) and analyses are colored according to their ^{207}Pb corrected apatite U-Pb age based on the sample's unique discordia. Solid black lines in the spiderplots are whole rock REE patterns. Circles in the radial plots (Vermeesch 2009) are colored according to their La/Lu_N ratio, with blank circles representing grains that no geochemical data was obtained.

4.4.3 Apatite and whole rock trace element results

All three volcanic samples (GM-03, GM-05, and GM-08) display comparable REE patterns with MREE showing 200 to 2000 the chondritic values (Figure 7). All three samples show an enrichment in LREE compared to MREE (La/Sm_N median values at 10.71, 2.78 and 2.38 , respectively) and a moderate negative Eu anomaly (Eu/Eu* median values at 0.55, 0.40 and 0.48, respectively). Sample GM-03 shows a relatively flat HREE trend (Dy/Yb_N ranging from 1.00 to 1.58) compared to samples GM-05 and GM-08 that are marked by more fractionated trends, with Dy/Yb_N ranges of 2.21-3.11 and 1.71-3.23, respectively. The whole rock REE profiles for each sample mirrors the apatite REE profile with an enrichment in LREE (GM-03, GM-05, and GM-08 La/Sm_N values of 4.57, 4.11, and 3.58, respectively) and depletion in HREE (GM-03, GM-05, and GM-08 Dy/Yb_N values of 1.23, 1.30, and 1.30, respectively), but with a more modest depletion in Eu (GM-03, GM-05, and GM-08 Eu/Eu* values of 0.77, 0.73, and 0.74, respectively, Figure 6-7). All three samples show very little variation between individual grain REE concentrations (Figure 6-7).

5 Discussion

The combination of apatite U-Pb dating, fission-track thermochronology, and apatite and whole rock trace element analysis, applied to well constrained tectonic environments across the North American Cordillera make it possible to distinguish thermal pathways and trace element patterns indicative of various crustal histories. Such discriminant chemical ratios for primary (geochemically representative of whole rock) *versus* secondary apatite (geochemically altered) are crucial for single-grain LA-ICP-MS U-Pb and FT analysis, as it is important to minimize the amount of material ablated as collecting the full range of REEs is material intensive. Finally, our results encourage the usage of apatite geochemistry to elucidate middle to upper crustal thermal histories across a range of cordilleran tectonic processes.

5.1 Primary *versus* secondary thermal history

By using apatite trace element chemistry it is possible to determine the nature of its host rock and to discuss their potential chemical reequilibration (e.g. Gillespie et al. 2018, O'Sullivan et al. 2020). Through trace element and REE composition; secondary (metamorphic or metasomatic) apatites can

be distinguished from their primary (magmatic) counterparts based on their depletion in LREE and/or HREE. These depleted trends are generally attributed to the growth of cogenetic mineral phases, with epidote and monazite sequestering LREE, and garnet sequestering HREE (Janots et al. 2008, El Korh et al. 2009, Henrichs et al. 2018, Glorie et al. 2019, Henrichs et al. 2019). Such metamorphic apatite composition is illustrated in samples KC82816-1, KC82816-2, and KC82816-3, marked by a larger spread of their $\sum$REE content but above all, showing concave downward REE pattern with unaffected MREE content, a large depletion of LREE and variable depletion of HREE (Figure 3). The apatite host-rock samples consist of an intermediate to granitic orthogneisses and a micaschist composition forming the cratonic basement which underwent medium- to high-grade metamorphic conditions (2-10 kbar and 400-800°C, Table 1 and Figure 3, e.g. Harms et al. 2004, Mueller et al. 2005). Additionally, apatites extracted from mylonitized granitic samples KJJ09-03 and MG1655 both display similar REE patterns, marked by moderate to major depletion in LREE. Depleting L- or H-REE alters the sum of an apatite's REE content, which is used as a sensitive proxy for distinction between igneous and metamorphic apatite; with the sum of REE in apatite decreasing with increasing metamorphic gradient (Figure 7A, e.g. Belousova et al. 2002*a*, El Korh et al. 2009, Henrichs et al. 2018).

Low LREE/MREE ratios (samples MG1655 and KJJ09-03) are interpreted as subsequent chemical re-equilibration during deformation and recrystallization at medium temperature conditions (~400-300°C); likely alongside the formation of LREE rich phases (Table 1 and Figure 5). More specifically, apatite recrystallization occurs simulatenously with monazite (LREE- and Th-rich) and/or epidote group minerals (LREE-rich and Sr-rich) in medium- to low-grade metamorphic felsic and mafic rocks (e.g. Grapes & Hoskin 2004, Glorie et al. 2019). These two reactions are a possible controls on the apatite geochemistry, with syn-crystallization of monazite influencing sample KC082816-2. Whereas epidote growth controls the apatite geochemistry observed in the mylonitic samples (MG1655 and KJJ09-03, Figure 7B). The Sr/Y ratio in apatite is variably used to distinguish igneous and metamorphic host rock or interpreted to indicate of increased fluid involvement (Nishizawa et al. 2005, Prowatke & Klemme 2006, Henrichs et al. 2018, Odlum & Stock Igneous apatites show strong negative correlation between Sr/Y and $\sum$REE due to the similar compatability of REE and Y in apatite (Figure 7A) as well as lower $\sum$REE and Sr/Y ratio values. These trends agree with the co-recrystallization of Ca-rich (and thus Sr-rich) phases like epidote during metamorphism.

The Th/U ratio in zircon is a reliable proxy to distinguish metamorphic and magmatic zircon (e.g. Rubatto 2002)an here we apply it to apatite. Cordilleran apatites from metamorphic samples displaying a decreasing trend in Th/U coeval with decreasing La/Sm_N (Figure 7B) attributed to the co-recrystallization of

Th-rich phases like monazite. Uranium depletion has been observed in many metamorphic apatites (O'Sullivan et al. 2018, Henrichs et al. 2018, 2019), however, apatites in these studies were sourced from coarse-grained rocks. Large diffusion domains in coarse grained rocks can obscure precise metamorphic processes. There was no noticeable difference between U concentrations of metamorphic (e.g. sample KC82816-1 yielded 3-66 ppm) and igneous apatite (e.g. sample GM-03 yielded 3-15 ppm, Supplementary Table 1) in this study. Rather, U abundances are thought to be controlled by the nature and composition of the host whole rock U concentration. As this study largely focuses on felsic crustal rocks, little variation between samples is expected (O'Sullivan et al. 2020).

The apatites extracted from mylonitized granitic samples (KJJ09-03 and MG1655) show a notable enrichment in HREE uncorrelated to the whole rock composition (Figure 5J). A possible source of these HREE could be the retrogression of garnet, destabilized during low-grade metamorphism (Rubatto 2002, Rubatto & Hermann 2007, Odlum & Stockli 2020). Here we suggest that the retrogression of garnet during low-grade metamorphism is losing HREE for which apatite is providing a sink whilst undergoing diffusion between ~450-375°C (Figure 7A and Supplementary File 8).

Several authors use the Eu anomaly as a proxy to track oxygen fugacity in igneous systems (e.g. Bau 1991, Trail et al. 2012). In our study, the variability in Eu anomaly is likely related to preexisting Eu anomaly in the whole rock composition (e.g. Figure 5E and H). This is supported by single sample inter-grain variability in the Eu anomaly, Sr/Y, and sumREE for either magmatic or metamorphic host rocks (Figure 7A and C). Thus, the Eu anomaly for a given apatite is likely inherited from the source composition of the parental magma of its respective rock and associated pre- or cogenetic crystallization of plagioclase during apatite crystallization (Figure 7D, e.g. Lu et al. 2016, O'Sullivan et al. 2020). This, further emphasizes the applicability of Eu anomaly in individual apatite grains to decipher its host rock composition, degree of crustal reworking, and depth of magmatic source (e.g. Henrichs et al. 2018, Nathwani et al. 2020).

Samples MG3150 and MG2465 both display low LREE/HREE ratios and flat REE patterns that are typical of metamorphic apatite, despite both rocks coming from weakly metamorphosed and non-metamorphosed rocks, an orthogneiss and granodiorite, respectively (Figure 5 and Table 1). This suggests that it is possible to have some degree of diffusion of REEs in apatite at temperatures sufficient for thermally-activated volume diffusion, but without causing the rock and apatites to undergo metamorphic recrystallisation, demonstrating the applicability of apatite as a useful tool for tracking petrochronological

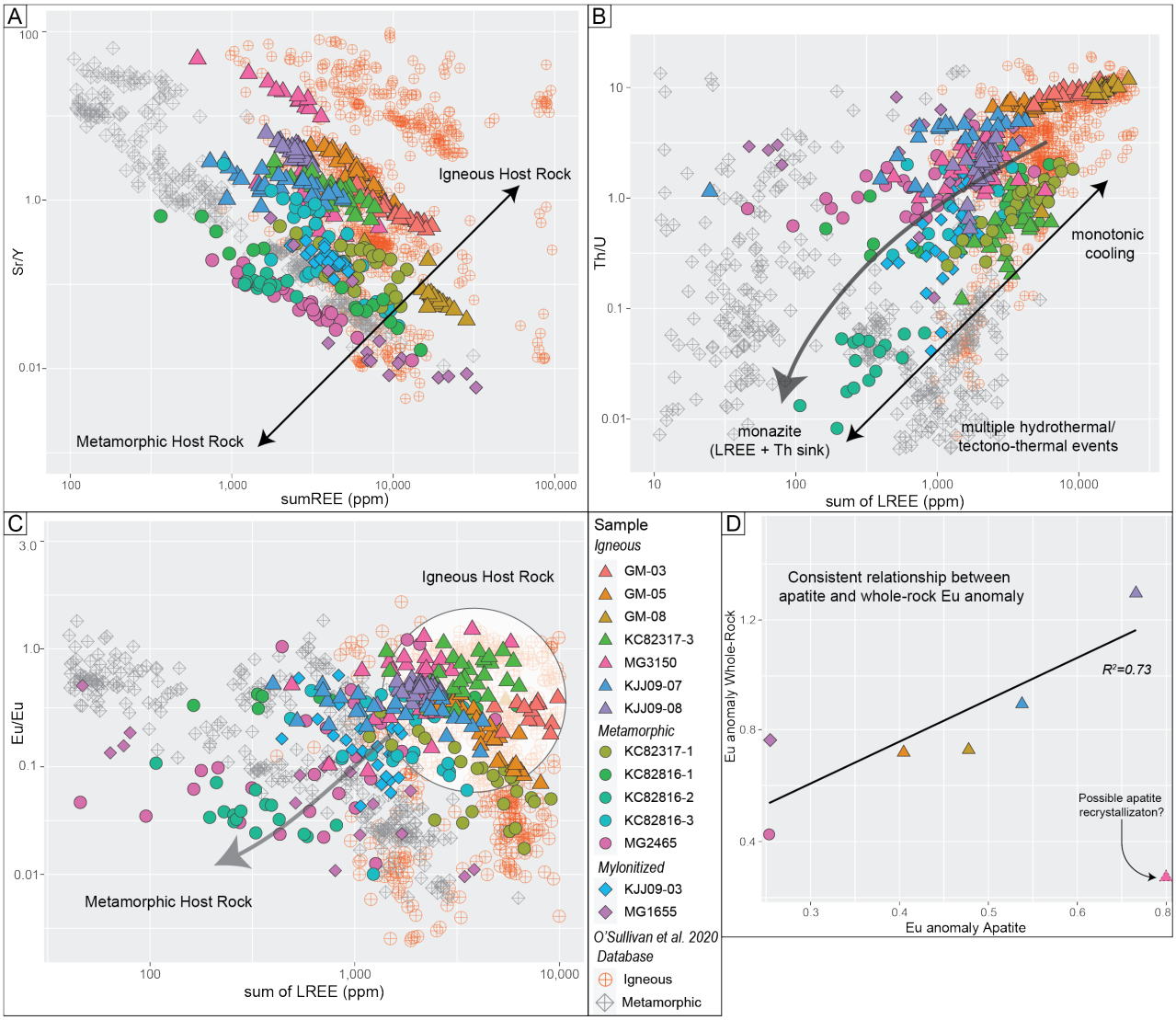

Figure 7: Apatite geochemistry diagrams plotting A) Sr/Y against sum of rare earth elements (REE), B) Th/U against sum of light REEs (La-Nd), C) Eu/Eu* against sum of light REEs (La-Nd) and D) Eu/Eu* whole rock against Eu/Eu* apatite. Plotted for comparison are igneous and metamorphic apatite from O'Sullivan et al. (2020)'s apatite geochemistry database.

processes (Smye et al. 2018).

The ratio of light to heavy REE can be used to distinguish between primary, igneous apatite which is reflective of its original melt conditions and metamorphic apatite or apatite which has experienced subsequent geochemical alteration. For detailed discrimination of apatite geochemistry, the reader is referred to O'Sullivan et al. (2020) and references therein. High La/Lu_N ratios (>50) correlate with apatite of igneous origin (i.e. samples KC82317-1, KC82317-3, KJJ09-07, KJJ09-08, GM-03, GM-05, and GM-08) and low La/Lu_N ratios (<10) define apatite which has undergone either metamorphic recrystallization or mid-crustal fluid alteration (i.e. samples KC82816-1, KC82816-2, KC82816-3, KJJ09-03, MG3150, MG2465, and MG1655, Table 1 and Figures 3-5). Among primary igneous apatite, the samples for which whole rock were obtained (KJJ09-08, GM-03, GM-05, and GM-08) show that primary igneous apatite REE patterns are in good agreement with associated whole rock REE patterns but with far greater $\sum$REE values (Figure 4 and 6). Thus, apatite with high La/Lu_N ratio can be used to investigate the composition of the primary melt from which it equilibrates. Finally, the range of magmatic and metamorphic processes observable in apatite indicates that apatite geochemistry has the potential to provide complementary information on melt-forming conditions in conjunction with commonly used accessory minerals such as monazite, titanite and zircon (e.g., Kylander-Clark et al. 2013, Chapman et al. 2016, Kirkland et al. 2020).

5.2 Link between *in situ* geochemical signature and cooling mechanisms

Apatite trace and REE geochemistry reflects crystallization processes as well as medium-temperature crustal processes such as exhumation, hydrothermal alteration, and magma-storage (e.g., Glorie et al. 2019, Odlum & Stockli 2020, Nathwani et al. 2020). However, apatite trace and REE geochemistry can also provide insight into low-temperature exhumation mechanisms. Specifically, the intra-sample variation in single grain trace elements suggests that REEs are undergoing modification via hydrothermal activity at temperatures that are not resetting the apatite U-Pb system. Here we integrate AUPb, AFT, and trace and REE geochemistry from well constrained tectonic settings in order to define the thermo-tectonic pathway of apatite from the mid- to upper crust (Figure 8 and 9)

5.2.1 Volcanic cooling

The combined U-Pb, FT, and trace element approach was applied to three volcanic rock samples in the Galiuro Mountains ignimbrite complex (Table 1). The Galiuro Mountains ignimbrite complex is dated at

its base as Oligocene (27.3 Ma, Dickinson 1991), which within error of the Eocene-Oligocene apatite U-Pb and FT dates obtained in this study (41 ± 12 Ma, 28 ± 31 Ma, and 29 ± 12 Ma, Table 4 and Figure 6). All three volcanic samples display high uncertainty which is likely a product of their rapid crystallization, cooling, and geochemical homogeneity making it difficult to fit a non-radiogenic Pb discordia, however, as they are within error of published constraints we view their ages as representative. The REE patterns obtained for the Galiuro Mountain samples (GM-03, GM-05, and GM-08) all display little intra-sample single-grain variation and give profiles which mirror their respective whole rock geochemistry (Figure 7 and Figure 8). In addition, elevated Th/U and La/Sm_N ratios with low intragrain variability are characteristic of the volcanic rock samples (Figure 7C). The Galiuro Mountains ignimbrite complex is interpreted to be rapidly cooled from the melt during several Oligocene eruptions and has remained undisturbed at surface temperature until present day (e.g., Dickinson 1991, Arca et al. 2010). Thus, we suggest that the consistency between apatite U-Pb and FT ages, combined with elevated Th/U and a homogeneous trace and REEs across single-grain analyses is indicative of a thermal history characterized by rapid cooling from ~575°C to upper crustal temperatures of ~60°C without any secondary thermal or fluid alteration (Figure 9).

5.2.2 Laramide intrusions

A relationship between medium to low temperature cooling and trace elements is also observed in Laramide-aged intrustions from the Catalina Mountain. Sample KJJ09-08 was collected from granite which yields a zircon U-Pb age of 73 ± 2 Ma which is in close agreement with the apatite U-Pb age of 62 ± 21 Ma and is consistent with the apatite fission-track age of 41 ± 6 Ma, suggesting a single, monotonic cooling history (Table 4 and Figure 4, Terrien 2012, Fornash et al. 2013). The close agreement of these high to low temperature thermochronometric systems is complimented by a homogeneous trace and REE distribution and consistently high Th/U and La/Lu ratios Figure 7B-8. This further emphasizes that homogeneous, elevated Th/U and La/Lu_N ratios is indicative of a monotonic cooling pathway to the upper crust (Figure 9).

Sample KJJ09-07 was collected from a granodiorite which yielded a zircon U-Pb age of 69 ± 3 Ma, a relatively precise apatite U-Pb age of 40 ± 4 Ma, and younger 24 ± 2 Ma apatite-fission track cooling age (Table 4 and Figure 4, Terrien 2012, Fornash et al. 2013). These ages are in relatively close agreement and could be interpreted as a single cooling history with discrete cooling pulses, however, the single-grain spread in apatite trace and REE (Th/U and La/Lu_N, Figure 7-8) suggests that this sample underwent

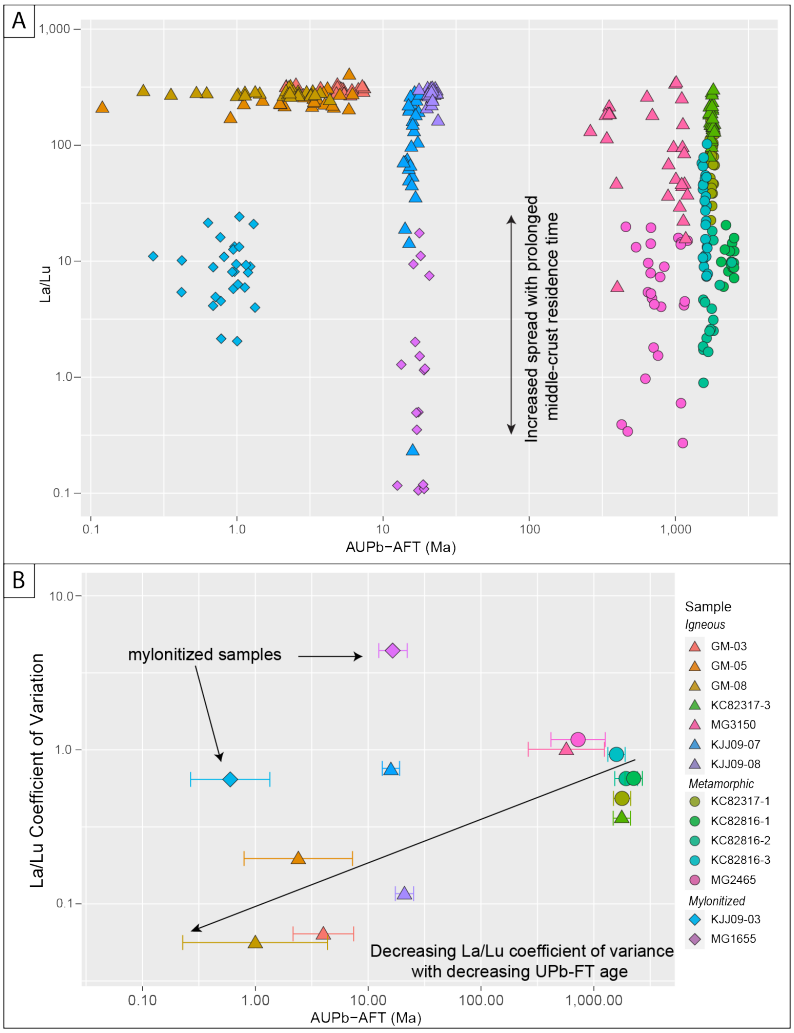

Figure 8: Plots showing A) Log-log of apatite U-Pb age minus apatite fission-track age against La/Lu_N ratio, and B) Log-log of apatite U-Pb age minus apatite fission-track age against the median La/Lu_N ratio divided by the standard deviation. Samples which have experienced protracted residence in the middle-crust correlate with an increased spread of La/Lu_N ratios and higher La/Lu_N coefficient of variance.

an additional period of mid-crust alteration. Expanding on this, previous studies in the Catalina Core Complex have found a distinctive phase of Eocene-aged dikes throughout the range and Eocene zircon rim growth in the Laramide-aged intrusions (Fornash et al. 2013, Ducea et al. 2020). These samples contain moderate to high Th/U and La/Sm_N ratios (Figure 7C). Increased magmatic activity in the Eocene would have elevated the geothermal gradient and resulted in hydrothermal fluids which percolated and cooled through the middle-to-upper crust resulting in a varying degree of alteration across single-grain REE geochemistry, but insufficient to deviate the apatite chemistry from the whole rock REE pattern (Figures 4 and 8). Thus, the variance in single-grain REE geochemistry, and Th/U, La/Sm_N, the La/Lu_N ratios, can be indicative of fluid alteration, medium-temperature thermal perturbation or prolonged residence (Figure 9).

5.2.3 Metamorphic core complex and detachment faulting

Apatite U-Pb dating has been shown to constrain the timing of faulting along major detachment fault systems as the apatite U-Pb temperature window (350-550°C) is ideally suited to constraining crustal evolution through the brittle-ductile transition zone (~10 km depth, e.g., Odlum & Stockli 2020). Samples KJJ09-03 and MG1655 were both collected from mylonitized basement exposed along the base of the Catalina and Pinaleño Core Complexes, respectively (Table 1). Zircon U-Pb dates from sample KJJ09-03 constrain crystallization to 56.6 ± 3 Ma (Fornash et al. 2013) whereas sample MG1655 is mapped as Paleoproterozoic in age (Johnson & Arca 2010). Apatite U-Pb ages from those same samples define a discordia age of 21 ± 5 Ma for sample KJJ09-03 and 39 ± 7 Ma for sample MG1655. Albeit with relatively large uncertainty (Figure 5), the AUPb age for sample KJJ09-03 is within error of the age for the onset of detachment extension of *ca.* 26.4 Ma along the Catalina detachment and sample MG1655 is slightly older than the *ca.* 29 Ma constraint placed along the Pinaleño detachment (Long et al. 1995, Peters et al. 2003, Terrien 2012). The close match between AUPb age and the hypothesized timing of mylonitization emphasizes the applicability of the apatite U-Pb to constrain timing of detachment faulting (Odlum & Stockli 2020). The REE geochemistry for both mylonitized samples display significantly altered profiles (depleted in LREE and enriched in HREE) when compared to their respective whole rock REE patterns (Henrichs et al. 2018), suggesting that the AUPb ages are reflective of apatite recrystallization during mylonitization. Zircons from sample KJJ09-3 displayed disturbed Hf isotopic values, which were attributed to mobilization of REEs during mylonitization (Fornash et al. 2013) demonstrating the distinct AUPb age and associated geochemistry are indicative of detachment faulting. Further, the La/Lu_N ratio

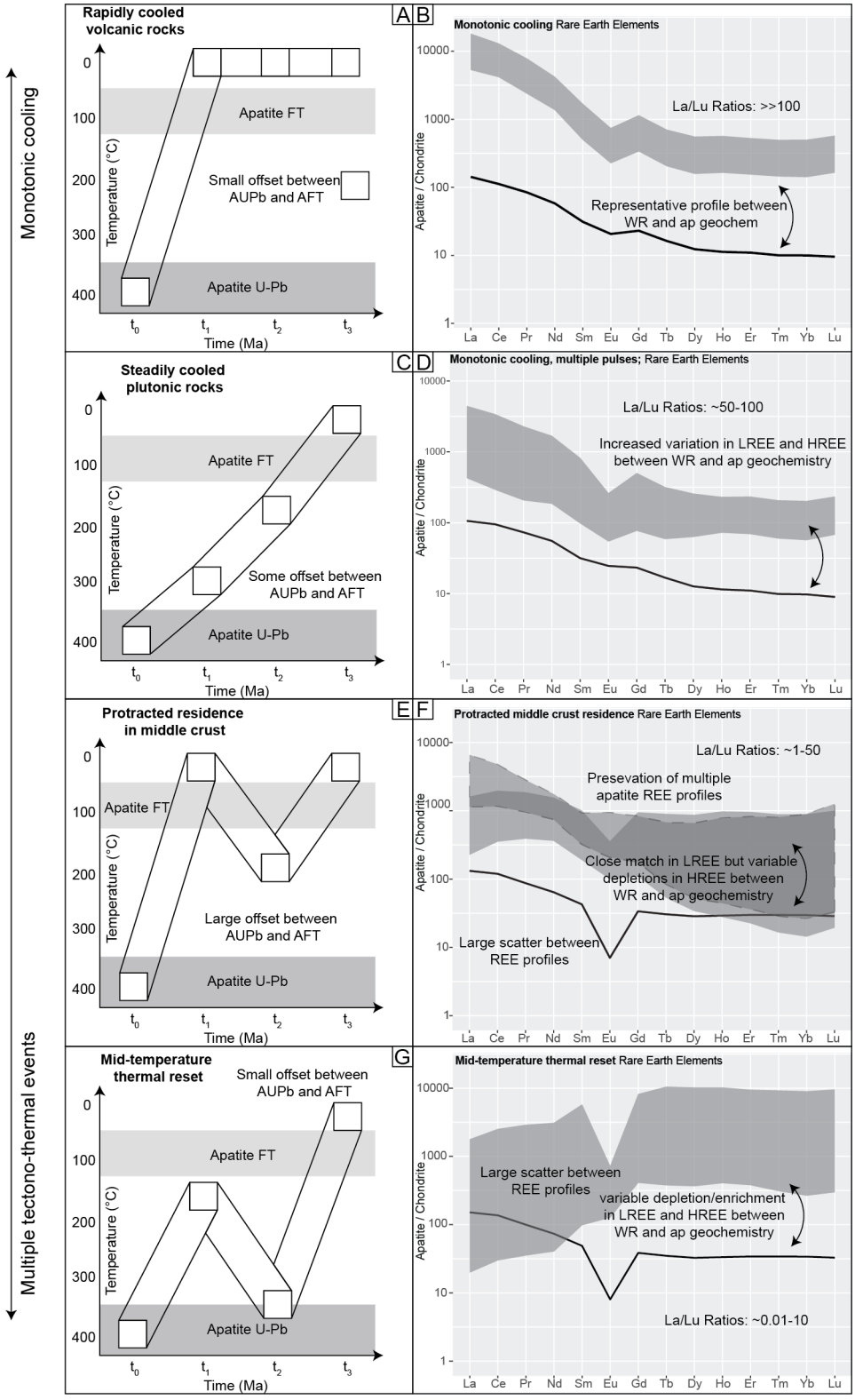

Figure 9: A summary diagram illustrating the relationship between apatite U-Pb (AUPb), apatite (ap) and whole rock (wr) trace and rare earth element (REE) geochemistry, and apatite fission-track (AFT) across four Cordilleran tectonic terranes.

is far more consistent across single-grains for sample KJJ09-03 than MG1655 (Figure 8), suggesting a prolonged residence time in the middle crust leads to increased variation in apatite geochemistry.

Research from a Metamorphic Core Complex in the Pyrenees found that AUPb ages and geochemistry were able to constrain multiple phases of hydrothermal fluid involvement associated with fault movement (Odlum & Stockli 2020). In their study, the upper and lower limits of the discordia spread dated the crystallization and exhumation ages, respectively (Odlum & Stockli 2020). In contrast, the two samples from beneath the detachment in the Pinaleño Mountains MCC (MG3150 and MG2465) preserved two distinctive discordia ages of *ca.* 1100 Ma, and *ca.* 400 Ma (Figure 5). These ages considerably predate the onset of the Oligocene Pinaleño detachment (29 Ma) and are temporally unrelated to Paleogene phase of exhumation along a detachment fault (Long et al. 1995). However, the *ca.* 1.1 Ga apatite U-Pb age is within error of Rb-Sr whole rock and baddeleyite U-Pb of dikes within the Pinaleño Mountains MCC (Swan 1976, Bright et al. 2014). Thus, we suggest that the younger discordia age relate to a subsequent period of magmatism or hydrothermal flux in the region (Odlum & Stockli 2020). Further, the preservation of multiple apatite U-Pb discordia within a single sample expands the range of potential petrochronology applications for apatite (Figure 9, Garber et al. 2017, Smye et al. 2018). Finally, both MG3150 and MG2465 demonstrate a broad range of Th/U, La/Sm_N, and La/Lu_N ratios, which could be indicative of either protracted residence in the middle crust or due to multiple emplacement stages during associated magmatic activity (Figure 7 and 8).

5.2.4 Basement cored uplifts

Previous studies have attempted to elucidate long-term cooling and exhumation from cratonic environments, finding that cratonic settings preserve distinct, stable low-temperature thermal histories (e.g., Flowers et al. 2006, Hall et al. 2018, Kohn & Gleadow 2019, McDannell et al. 2019). Cratonic basement exhumed along basement cored uplifts (KC82317-1, KC82317-3, KC82816-1, KC82816-2, and KC82816-3) all record Cretaceous AFT ages, suggesting that unlike cratonic environments in the Canadian Shield, South Australia and Baffin Island, the western Wyoming Craton experienced sufficient burial to reset the AFT low-temperature thermochronometer prior to the onset of the Laramide orogeny (Orme et al. 2016). Apatite U-Pb ages from the western Wyoming craton yield three discordant ages at*ca.* 2.4, *ca.* 1.8, and *ca.* 1.6 Ga (Figure 3).

Samples KC82317-1 and KC82317-3 display REE patterns that are indicative of primary igneous apatite (O'Sullivan et al. 2018, Gillespie et al. 2018) and their AUPb ages of *ca.* 1.8 Ga are within error of

zircon U-Pb and hornblende and biotite $^{40}Ar/^{39}Ar$ ages obtained from the Little Belt Mountains (Mueller et al. 2002, Holm & Schneider 2002, Foster et al. 2006). Therefore, we interpret these rocks (KC82317-1 and KC82317-3) to have remained at middle-to-upper crustal temperature from the Paleoproterozoic. This protracted thermo-tectonic history is reflected in the apatite REE composition (Figure 7), with high single-grain REE variability, low Th/U concentrations and a high La/Lu coefficient of variance ($CV = (\sigma/\mu) * 100$, Figures 3, 7C and 8).

Similar to the two Little Belt samples, sample KC82816-2 (Gravelly Range, Montana, Table 1) preserves an AUPb age of *ca.* 1.8 Ga (Figure 3). However, the concave REE pattern suggests that sample KC82816-2 underwent metamorphism during the Little Belt arc accretion at *ca.* 2.0-1.8 Ga (e.g., Foster et al. 2006, Whitmeyer & Karlstrom 2007). In contrast, the nearby sample KC82816-1 preserves an Archean age of *ca.* 2.4 Ga and an apatite REE pattern indicative of meta-pelitic rocks (Henrichs et al. 2018), suggesting that the apatite U-Pb age records evidence of cratonic assembly along the western boundary of the Wyoming Craton (Kellogg et al. 2003, Mueller & Frost 2006). Sample KC82816-3 records the youngest cratonic age of *ca.* 1.6 Ga, these form a single discordia and a low La/Lu ratio (Figure 8). The 1.6 Ga discordia age likely reflects a widespread tectono-thermal event along southwestern Montana between *ca.* 1.65-1.63 Ga (Mueller et al. 2005, Foster et al. 2006), which would have reset the apatite U-Pb chronometer. However, sample KC82816-3 preserves both an igneous and metamorphic REE pattern (Henrichs et al. 2018), suggesting that thermal conditions were not sufficient to completely re-equilibrate the apatite and the sample underwent selective alteration in response to hydrothermal fluid interaction (Figure 3 and Supplementary File 9).

Finally, samples KC82816-1, KC82816-2, and KC82816-3 (Gravelly Range, Montana, Table 1) all display low La/Lu and Th/U ratios, relatively high La/Lu coefficient of variance, and high variability along single-grain apatite REE patterns (Figure 3 and 7). Considering that this region of the Wyoming Craton is interpreted to have undergone very little exhumation since the Proterozoic (Foster et al. 2006, Whitmeyer & Karlstrom 2007), and the low-temperature thermochronometric systems are completely reset in the Cretaceous (Table 3), we suggest that the high La/Lu coefficient of variance and variable apatite REE patterns are evidence for protracted residence in the middle crust (Figure 9).

6 Conclusions

Through the combined application of apatite U-Pb and FT thermochronology with *in situ* and whole rock trace elemental geochemistry this study shows the viability of this petrochronological and thermochronological approach on a range of high to low temperature crustal settings. We demonstrate that the REE patterns and the La/Lu_N ratio can be interpreted as indicators to whether an apatite grain preserves a primary (whole rock representative; typically La/Lu_N >50) or secondary (geochemically modified; typically La/Lu_N <50)) thermal history. If the apatite geochemistry preserves a primary thermal history, then apatite geochemistry acts as a representative record of whole rock geochemistry similar to other commonly used accessory minerals. Apatite geochemistry applied to extrusive volcanic rocks demonstrates that consistent single-grain REE patterns reflect monotonic cooling. In contrast, samples which have undergone medium temperature (>250°C) thermal perturbation or samples that experience protracted residence in the middle crust host considerable single-grain REE variation. Thus, in absence of double dating, homogeneous intergrain REEs and elevated Th/U and La/Lu_N ratios are indicative of a monotonic cooling pathway through the upper crust. We further show the utility of apatite U-Pb thermochronology in constraining the timing of detachment faulting (sensu Odlum & Stockli 2020). Finally, apatite geochemistry has the potential to be an important complementary indicator of melt-forming conditions. Applied in conjunction with other commonly used accessory minerals (monazite, titanite, and zircon), the complex relationship between apatite thermochronology and geochemistry expands the applicability of apatite as a middle-crust thermochronometer.

7 Acknowledgements

Daniel Alberts is thanked for his work in establishing the apatite U-Pb and trace element method at the University of Arizona. James Worthington is thanked for his assistance with thin-section mineral identification. Reviewers Margret Odlum and David Chew, and editor Catherine Chauval are thanked for their insightful comments which improved the manuscript. Barbara Carrapa acknowledges US National Science Foundation grant EAR Tectonics 1919179. Mihai N. Ducea acknowledges US National Science Foundation grant EAR 1725002 and the Romanian Executive Agency for Higher Education, Research, Development and Innovation Funding project PN-III-P4-ID-PCCF-2016-0014. George E. Gehrels acknowledges US National Science Foundation EAR 1649254 for support of the Arizona LaserChron Center. Antoine Triantafyllou is a FRS-FNRS post-doctoral research fellow for the PROBARC project (Grant

CR n°1. B. 414.20F). Antoine Triantafyllou thanks the Rotary Club de Mons and the University of Mons for providing their financial support via the Pierre Jacobs post-doctoral grant (2018).

References

Arca, M. S., Kapp, P. & Johnson, R. A. (2010), 'Cenozoic crustal extension in southeastern Arizona and implications for models of core-complex development', *Tectonophysics* **488**(1), 174 – 190. Extensional Tectonics in the Basin and Range, the Aegean, and Western Anatolia.
URL: *http://www.sciencedirect.com/science/article/pii/S0040195110001435*

Atwater, T. (1970), 'Implications of Plate Tectonics for the Cenozoic Tectonic Evolution of Western North America', *GSA Bulletin* **81**(12), 3513–3536.
URL: *https://doi.org/10.1130/0016-7606(1970)81[3513:IOPTFT]2.0.CO;2*

Balica, C., Ducea, M., Gehrels, G., Kirk, J., Roban, R., Luffi, P., Chapman, J., Triantafyllou, A., Guo, J., Stoica, A., Ruiz, J., Balintoni, I., Profeta, L., Hoffman, D. & Petrescu, L. (2020), 'A zircon petrochronologic view on granitoids and continental evolution', *Earth and Planetary Science Letters* **531**, 116005.
URL: *http://www.sciencedirect.com/science/article/pii/S0012821X19306971*

Bau, M. (1991), 'Rare-earth element mobility during hydrothermal and metamorphic fluid-rock interaction and the significance of the oxidation state of europium', *Chemical Geology* **93**(3), 219 – 230.
URL: *http://www.sciencedirect.com/science/article/pii/0009254191901158*

Behr, W. M. & Smith, D. (2016), 'Deformation in the mantle wedge associated with Laramide flat-slab subduction', *Geochemistry, Geophysics, Geosystems* **17**(7), 2643–2660.
URL: *https://agupubs.onlinelibrary.wiley.com/doi/abs/10.1002/2016GC006361*

Belousova, E. A., Griffin, W. L., O'Reilly, S. Y. & Fisher, N. I. (2002*a*), 'Apatite as an indicator mineral for mineral exploration: trace-element compositions and their relationship to host rock type', *Journal of Geochemical Exploration* **76**(1), 45 – 69.
URL: *http://www.sciencedirect.com/science/article/pii/S0375674202002042*

Belousova, E. K., Griffin, W. L., O'Reilly, S. Y. & Fisher, N. L. (2002*b*), 'Igneous zircon: trace element composition as an indicator of source rock type', *Contributions to mineralogy and petrology* **143**(5), 602–622.

Best, M. G., Barr, D. L., Christiansen, E. H., Gromme, S., Deino, A. L. & Tingey, D. G. (2009), 'The Great Basin Altiplano during the middle Cenozoic ignimbrite flareup: insights from volcanic rocks', *International Geology Review* **51**(7-8), 589–633.
URL: *https://doi.org/10.1080/00206810902867690*

Best, M. G., Christiansen, E. H., de Silva, S. & Lipman, P. W. (2016), 'Slab-rollback ignimbrite flareups in the southern Great Basin and other Cenozoic American arcs: A distinct style of arc volcanism', *Geosphere* **12**(4), 1097–1135.
URL: *https://doi.org/10.1130/GES01285.1*

Bird, P. (1979), 'Continental delamination and the Colorado Plateau', *Journal of Geophysical Research: Solid Earth* **84**(B13), 7561–7571.
URL: *https://agupubs.onlinelibrary.wiley.com/doi/abs/10.1029/JB084iB13p07561*

Bird, P. (1998), 'Kinematic history of the Laramide orogeny in latitudes 35°–49°N, western United States', *Tectonics* **17**(5), 780–801.
URL: *https://agupubs.onlinelibrary.wiley.com/doi/abs/10.1029/98TC02698*

Blackburn, T., Bowring, S. A., Schoene, B., Mahan, K. & Dudas, F. (2011), 'U-Pb thermochronology: creating a temporal record of lithosphere thermal evolution', *Contributions to Mineralogy and Petrology* **162**(3), 479–500.
URL: *https://doi.org/10.1007/s00410-011-0607-6*

Braun, J., Van Der Beek, P. & Batt, G. (2006), *Quantitative thermochronology: numerical methods for the interpretation of thermochronological data*, Cambridge University Press.

Bright, R. M., Amato, J. M., Denyszyn, S. W. & Ernst, R. E. (2014), 'U-Pb geochronology of 1.1 Ga diabase in the southwestern United States: Testing models for the origin of a post-Grenville large igneous province', *Lithosphere* **6**(3), 135–156.
URL: *https://doi.org/10.1130/L335.1*

Brown, W. G. (1988), Deformational style of Laramide uplifts in the Wyoming foreland, *in* 'Interaction of the Rocky Mountain Foreland and the Cordilleran Thrust Belt', Geological Society of America.
URL: *https://doi.org/10.1130/MEM171-p1*

Bruand, E., Fowler, M., Storey, C. & Darling, J. (2017), 'Apatite trace element and isotope applications to petrogenesis and provenance', *American Mineralogist* **102**(1), 75 – 84.

Bruand, E., Storey, C. & Fowler, M. (2016), 'An apatite for progress: Inclusions in zircon and titanite constrain petrogenesis and provenance', *Geology* **44**(2), 91–94.
URL: *https://doi.org/10.1130/G37301.1*

Burchfiel, B. C., Cowan, D. S. & Davis, G. A. (1992), Tectonic overview of the Cordilleran orogen in the western United States, *in* 'The Cordilleran Orogen', Geological Society of America, pp. 407 – 480.
URL: *https://doi.org/10.1130/DNAG-GNA-G3.407*

Carrapa, B., DeCelles, P. G. & Romero, M. (2019), 'Early Inception of the Laramide Orogeny in Southwestern Montana and Northern Wyoming: Implications for Models of Flat-Slab Subduction', *Journal of Geophysical Research: Solid Earth* **124**(2), 2102–2123.
URL: *https://agupubs.onlinelibrary.wiley.com/doi/abs/10.1029/2018JB016888*

Carrapa, B., DeCelles, P., Reiners, P., Gehrels, G. & Sudo, M. (2009), 'Apatite triple dating and white mica 40Ar/39Ar thermochronology of syntectonic detritus in the Central Andes: A multiphase tectonothermal history', *Geology* **37**(5), 407–410.
URL: *https://doi.org/10.1130/G25698A.1*

Cassel, E. J., Smith, M. E. & Jicha, B. R. (2018), 'The Impact of Slab Rollback on Earth's Surface: Uplift and Extension in the Hinterland of the North American Cordillera', *Geophysical Research Letters* **45**(20), 10,996–11,004.
URL: *https://agupubs.onlinelibrary.wiley.com/doi/abs/10.1029/2018GL079887*

Chapman, J. B., Gehrels, G. E., Ducea, M. N., Giesler, N. & Pullen, A. (2016), 'A new method for estimating parent rock trace element concentrations from zircon', *Chemical Geology* **439**, 59 – 70.
URL: *http://www.sciencedirect.com/science/article/pii/S0009254116303060*

Cherniak, D., Lanford, W. & Ryerson, F. (1991), 'Lead diffusion in apatite and zircon using ion implantation and Rutherford Backscattering techniques', *Geochimica et Cosmochimica Acta* **55**(6), 1663 – 1673.
URL: *http://www.sciencedirect.com/science/article/pii/001670379190137T*

Chew, D. M., Babechuk, M. G., Cogné, N., Mark, C., O'Sullivan, G. J., Henrichs, I. A., Doepke, D. & McKenna, C. A. (2016), '(LA,Q)-ICPMS trace-element analyses of Durango and McClure Mountain

apatite and implications for making natural LA-ICPMS mineral standards', *Chemical Geology* **435**, 35 – 48.
URL: *http://www.sciencedirect.com/science/article/pii/S0009254116301590*

Chew, D. M. & Donelick, R. A. (2012), 'Combined apatite fission track and U-Pb dating by LA-ICP-MS and its application in apatite provenance analysis', *Quantitative mineralogy and microanalysis of sediments and sedimentary rocks: Mineralogical Association of Canada Short Course* **42**, 219–247.

Chew, D. M. & Spikings, R. A. (2015), 'Geochronology and Thermochronology Using Apatite: Time and Temperature, Lower Crust to Surface', *Elements* **11**(3), 189–194.
URL: *https://doi.org/10.2113/gselements.11.3.189*

Chew, D., O'Sullivan, G., Caracciolo, L., Mark, C. & Tyrrell, S. (2020), 'Sourcing the sand: Accessory mineral fertility, analytical and other biases in detrital U-Pb provenance analysis', *Earth-Science Reviews* **202**, 103093.
URL: *http://www.sciencedirect.com/science/article/pii/S0012825219305835*

Chew, D., Petrus, J. & Kamber, B. (2014), 'U–Pb LA–ICPMS dating using accessory mineral standards with variable common Pb', *Chemical Geology* **363**, 185 – 199.
URL: *http://www.sciencedirect.com/science/article/pii/S000925411300510X*

Cochrane, R., Spikings, R. A., Chew, D., Wotzlaw, J.-F., Chiaradia, M., Tyrrell, S., Schaltegger, U. & der Lelij, R. V. (2014), 'High temperature (>350°C) thermochronology and mechanisms of Pb loss in apatite', *Geochimica et Cosmochimica Acta* **127**, 39 – 56.
URL: *http://www.sciencedirect.com/science/article/pii/S0016703713006674*

Coney, P. J. (1978), Mesozoic-Cenozoic Cordilleran plate tectonics, *in* 'Cenozoic Tectonics and Regional Geophysics of the Western Cordillera', Geological Society of America, pp. 33–50.
URL: *https://doi.org/10.1130/MEM152-p33*

Coney, P. J. (1987), 'The regional tectonic setting and possible causes of cenozoic extension in the north american cordillera', *Geological Society, London, Special Publications* **28**(1), 177–186.
URL: *https://sp.lyellcollection.org/content/28/1/177*

Coney, P. J., Jones, D. L., Monger, J. W. H. et al. (1980), 'Cordilleran suspect terranes', *Nature* **288**(5789), 329–333.

Coney, P. J. & Reynolds, S. J. (1977), 'Cordilleran benioff zones', *Nature* **270**(5636), 403–406.

Constenius, K. N. (1996), 'Late Paleogene extensional collapse of the Cordilleran foreland fold and thrust belt', *GSA Bulletin* **108**(1), 20–39.
URL: *https://doi.org/10.1130/0016-7606(1996)108<0020:LPECOT>2.3.CO;2*

Constenius, K. N., Esser, R. P. & Layer, P. W. (2003), Extensional collapse of the charleston-nebo salient and its relationship to space-time variations in cordilleran orogenic belt tectonism and continental stratigraphy, *in* 'Cenozoic Systems of the Rocky Mountain Region', Rocky Mountain Section (SEPM),.

Coutand, I., Carrapa, B., Deeken, A., Schmitt, A. K., Sobel, E. R. & Strecker, M. R. (2006), 'Propagation of orographic barriers along an active range front: insights from sandstone petrography and detrital apatite fission-track thermochronology in the intramontane Angastaco basin, NW Argentina', *Basin Research* **18**(1), 1–26.
URL: *https://onlinelibrary.wiley.com/doi/abs/10.1111/j.1365-2117.2006.00283.x*

Creasey, S. C. & Krieger, M. H. (1978), 'Galiuro Volcanics, Pinal, Graham and Cochise counties, Arizona', *Journal of Research of the U.S. Geological Survey* **6**, 115–31.

Davis, G. H. (1980), Structural characteristics of metamorphic core complexes, southern Arizona, *in* 'Cordilleran Metamorphic Core Complexes', Geological Society of America, pp. 35–78.
URL: *https://doi.org/10.1130/MEM153-p35*

DeCelles, P. G. (2004), 'Late Jurassic to Eocene evolution of the Cordilleran thrust belt and foreland basin system, western USA', *American Journal of Science* **304**(2), 105–168.

DeCelles, P. G., Ducea, M. N., Kapp, P. & Zandt, G. (2009), 'Cyclicity in Cordilleran orogenic systems', *Nature Geoscience* **2**(4), 251–257.

Dewey, J. F. (1988), 'Extensional collapse of orogens', *Tectonics* **7**(6), 1123–1139.
URL: *https://agupubs.onlinelibrary.wiley.com/doi/abs/10.1029/TC007i006p01123*

Dickinson, W. R. (1991), Tectonic setting of faulted Tertiary strata associated with the Catalina core complex in southern Arizona, *in* 'Tectonic setting of faulted Tertiary strata associated with the Catalina core complex in southern Arizona', Geological Society of America.
URL: *https://doi.org/10.1130/SPE264-p1*

729 Dickinson, W. R. (2004), 'Evolution of the North American Cordillera', *Annual Review of Earth and*
730 *Planetary Sciences* **32**(1), 13–45.
731 **URL:** *https://doi.org/10.1146/annurev.earth.32.101802.120257*

732 Dickinson, W. R. & Lawton, T. F. (2001), 'Carboniferous to Cretaceous assembly and fragmentation of
733 Mexico', *GSA Bulletin* **113**(9), 1142–1160.
734 **URL:** *https://doi.org/10.1130/0016-7606(2001)113<1142:CTCAAF>2.0.CO;2*

735 Dickinson, W. R. & Snyder, W. S. (1978), Plate tectonics of the Laramide orogeny, *in* 'Laramide Folding
736 Associated with Basement Block Faulting in the Western United States', Geological Society of America.
737 **URL:** *https://doi.org/10.1130/MEM151-p355*

738 Dilek, Y. & Moores, E. M. (1999), 'A Tibetan model for the early Tertiary western United States', *Journal*
739 *of the Geological Society* **156**(5), 929–941.
740 **URL:** *https://jgs.lyellcollection.org/content/156/5/929*

741 Donelick, R. A. & Miller, D. S. (1991), 'Enhanced tint fission track densities in low spontaneous track
742 density apatites using 252Cf-derived fission fragment tracks: A model and experimental observations',
743 *International Journal of Radiation Applications and Instrumentation. Part D. Nuclear Tracks and*
744 *Radiation Measurements* **18**(3), 301 – 307.
745 **URL:** *http://www.sciencedirect.com/science/article/pii/135901899190022A*

746 Donelick, R. A., O'Sullivan, P. B. & Ketcham, R. A. (2005), 'Apatite Fission-Track Analysis', *Reviews in*
747 *Mineralogy and Geochemistry* **58**(1), 49.
748 **URL:** *http://dx.doi.org/10.2138/rmg.2005.58.3*

749 Ducea, M. N. & Chapman, A. D. (2018), 'Sub-magmatic arc underplating by trench and forearc materials
750 in shallow subduction systems; a geologic perspective and implications', *Earth-Science Reviews* **185**, 763
751 – 779.
752 **URL:** *http://www.sciencedirect.com/science/article/pii/S0012825218302666*

753 Ducea, M. N., Paterson, S. R. & DeCelles, P. G. (2015), 'High-Volume Magmatic Events in Subduction
754 Systems', *Elements* **11**(2), 99–104.
755 **URL:** *https://doi.org/10.2113/gselements.11.2.99*

Ducea, M. N., Triantafyllou, A. & Krcmaric, J. (2020), 'New Timing and Depth Constraints for the Catalina Metamorphic Core Complex, Southeast Arizona', *Tectonics* **39**(8), e2020TC006383. e2020TC006383 2020TC006383.

URL: *https://agupubs.onlinelibrary.wiley.com/doi/abs/10.1029/2020TC006383*

Ehlers, T. A. (2005), 'Crustal Thermal Processes and the Interpretation of Thermochronometer Data', *Reviews in Mineralogy and Geochemistry* **58**(1), 315–350.

URL: *https://doi.org/10.2138/rmg.2005.58.12*

El Korh, A., Schmidt, S. T., Ulianov, A. & Potel, S. (2009), 'Trace Element Partitioning in HP–LT Metamorphic Assemblages during Subduction-related Metamorphism, Ile de Groix, France: a Detailed LA-ICPMS Study', *Journal of Petrology* **50**(6), 1107–1148.

URL: *https://doi.org/10.1093/petrology/egp034*

Engebretson, D. C., Cox, A. & Gordon, R. G. (1985), Relative Motions Between Oceanic and Continental Plates in the Pacific Basin, *in* 'Relative Motions Between Oceanic and Continental Plates in the Pacific Basin', Geological Society of America.

URL: *https://doi.org/10.1130/SPE206-p1*

Erslev, E. A. (1993), Thrusts, back-thrusts and detachment of Rocky Mountain foreland arches, *in* C. J. Schmidt, R. B. Chase & E. A. Erslev, eds, 'Laramide basement deformation in the Rocky Mountain foreland of the western United States', Vol. 280, Geological Society America, p. 339–358.

Fitzgerald, P. G., Stump, E. & Redfield, T. F. (1993), 'Late Cenozoic Uplift of Denali and Its Relation to Relative Plate Motion and Fault Morphology', *Science* **259**(5094), 497–499.

URL: *https://science.sciencemag.org/content/259/5094/497*

Flowers, R., Bowring, S. & Reiners, P. (2006), 'Low long-term erosion rates and extreme continental stability documented by ancient (U-Th)/He dates', *Geology* **34**(11), 925–928.

URL: *https://doi.org/10.1130/G22670A.1*

Fornash, K. F., Patchett, P. J., Gehrels, G. E. & Spencer, J. E. (2013), 'Evolution of granitoids in the Catalina metamorphic core complex, southeastern Arizona: U–Pb, Nd, and Hf isotopic constraints', *Contributions to Mineralogy and Petrology* **165**(6), 1295–1310.

Foster, D. A., Mueller, P. A., Mogk, D. W., Wooden, J. L. & Vogl, J. J. (2006), 'Proterozoic evolution of the western margin of the Wyoming craton: implications for the tectonic and magmatic evolution of the northern Rocky Mountains', *Canadian Journal of Earth Sciences* **43**(10), 1601–1619.
URL: *https://doi.org/10.1139/e06-052*

Frost, C. D., Frost, B., Chamberlain, K. R. & Hulsebosch, T. P. (1998), 'The late archean history of the wyoming province as recorded by granitic magmatism in the wind river range, wyoming', *Precambrian Research* **89**(3), 145 – 173.
URL: *http://www.sciencedirect.com/science/article/pii/S030192689700082X*

Galbraith, R. F. (1981), 'On statistical models for fission track counts', *Journal of the International Association for Mathematical Geology* **13**(6), 471–478.
URL: *https://doi.org/10.1007/BF01034498*

Garber, J. M., Hacker, B. R., Kylander-Clark, A. R. C., Stearns, M. & Seward, G. (2017), 'Controls on Trace Element Uptake in Metamorphic Titanite: Implications for Petrochronology', *Journal of Petrology* **58**(6), 1031–1057.
URL: *https://doi.org/10.1093/petrology/egx046*

Gehrels, G. & Pecha, M. (2014), 'Detrital zircon U-Pb geochronology and Hf isotope geochemistry of Paleozoic and Triassic passive margin strata of western North America', *Geosphere* **10**(1), 49–65.
URL: *https://doi.org/10.1130/GES00889.1*

Gillespie, J., Glorie, S., Khudoley, A. K. & Collins, A. S. (2018), 'Detrital apatite U-Pb and trace element analysis as a provenance tool: Insights from the Yenisey Ridge (Siberia)', *Lithos* **314-315**, 140 – 155.
URL: *http://www.sciencedirect.com/science/article/pii/S0024493718301890*

Gleadow, A. J., Belton, D. X., Kohn, B. P. & Brown, R. W. (2002), 'Fission Track Dating of Phosphate Minerals and the Thermochronology of Apatite', *Reviews in Mineralogy and Geochemistry* **48**(1), 579.
URL: *+ http://dx.doi.org/10.2138/rmg.2002.48.16*

Gleadow, A. J. W., Duddy, I. R., Green, P. F. & Lovering, J. F. (1986), 'Confined fission track lengths in apatite: a diagnostic tool for thermal history analysis', *Contributions to Mineralogy and Petrology* **94**(4), 405–415.
URL: *https://doi.org/10.1007/BF00376334*

Glorie, S., Jepson, G., Konopelko, D., Mirkamalov, R., Meeuws, F., Gilbert, S., Gillespie, J., Collins, A. S., Xiao, W. J., Dewaele, S. & De Grave, J. (2019), 'Thermochronological and geochemical footprints of post-orogenic fluid alteration recorded in apatite: Implications for mineralisation in the Uzbek Tian Shan', *Gondwana Research* **71**, 1 – 15.
URL: *http://www.sciencedirect.com/science/article/pii/S1342937X19300498*

Grapes, R. H. & Hoskin, P. W. O. (2004), 'Epidote Group Minerals in Low–Medium Pressure Metamorphic Terranes', *Reviews in Mineralogy and Geochemistry* **56**(1), 301–345.
URL: *https://doi.org/10.2138/gsrmg.56.1.301*

Grimes, C. B., Wooden, J. L., Cheadle, M. J. & John, B. E. (2015), '"Fingerprinting" tectono-magmatic provenance using trace elements in igneous zircon', *Contributions to Mineralogy and Petrology* **170**(5-6), 46.

Hall, J. W., Glorie, S., Reid, A. J., Collins, A. S., Jourdan, F., Danišík, M. & Evans, N. (2018), 'Thermal history of the northern Olympic Domain, Gawler Craton; correlations between thermochronometric data and mineralising systems', *Gondwana Research* **56**, 90 – 104.
URL: *http://www.sciencedirect.com/science/article/pii/S1342937X18300030*

Harms, T. A., Brady, J. B., Burger, H. R. & Cheney, J. T. (2004), Advances in the geology of the Tobacco Root Mountains, Montana, and their implications for the history of the northern Wyoming province, *in* 'Precambrian Geology of the Tobacco Root Mountains, Montana', Geological Society of America.
URL: *https://doi.org/10.1130/0-8137-2377-9.227*

Hasebe, N., Barbarand, J., Jarvis, K., Carter, A. & Hurford, A. J. (2004), 'Apatite fission-track chronometry using laser ablation ICP-MS', *Chemical Geology* **207**(3), 135 – 145.
URL: *http://www.sciencedirect.com/science/article/pii/S0009254104000427*

Henderson, L. J., Gordon, R. G. & Engebretson, D. C. (1984), 'Mesozoic aseismic ridges on the farallon plate and southward migration of shallow subduction during the laramide orogeny', *Tectonics* **3**(2), 121–132.
URL: *https://agupubs.onlinelibrary.wiley.com/doi/abs/10.1029/TC003i002p00121*

Henrichs, I. A., Chew, D. M., O'Sullivan, G. J., Mark, C., McKenna, C. & Guyett, P. (2019), 'Trace Element (Mn-Sr-Y-Th-REE) and U-Pb Isotope Systematics of Metapelitic Apatite During Progressive

Greenschist- to Amphibolite-Facies Barrovian Metamorphism', *Geochemistry, Geophysics, Geosystems* **20**(8), 4103–4129.
URL: *https://agupubs.onlinelibrary.wiley.com/doi/abs/10.1029/2019GC008359*

Henrichs, I. A., O'Sullivan, G., Chew, D. M., Mark, C., Babechuk, M. G., McKenna, C. & Emo, R. (2018), 'The trace element and U-Pb systematics of metamorphic apatite', *Chemical Geology* **483**, 218 – 238.
URL: *http://www.sciencedirect.com/science/article/pii/S000925411730712X*

Hoffman, P. F. (1988), 'United plates of america, the birth of a craton: Early proterozoic assembly and growth of laurentia', *Annual Review of Earth and Planetary Sciences* **16**(1), 543–603.

Holm, D. & Schneider, D. (2002), '40Ar/39Ar evidence for ca. 1800 Ma tectonothermal activity along the Great Falls tectonic zone, central Montana', *Canadian Journal of Earth Sciences* **39**(12), 1719–1728.
URL: *https://doi.org/10.1139/e02-069*

Horne, A. M., van Soest, M. C. & Hodges, K. V. (2019), 'U/Pb and (U-Th-Sm)/He "double" dating of detrital apatite by laser ablation: A critical evaluation', *Chemical Geology* **506**, 40 – 50.
URL: *http://www.sciencedirect.com/science/article/pii/S0009254118305898*

Humphreys, E. (2009), Relation of flat subduction to magmatism and deformation in the western United States, *in* 'Backbone of the Americas: Shallow Subduction, Plateau Uplift, and Ridge and Terrane Collision', Geological Society of America.
URL: *https://doi.org/10.1130/2009.1204(04)*

Inglis, E. C., Creech, J. B., Deng, Z. & Moynier, F. (2018), 'High-precision zirconium stable isotope measurements of geological reference materials as measured by double-spike MC-ICPMS', *Chemical Geology* **493**, 544 – 552.
URL: *http://www.sciencedirect.com/science/article/pii/S0009254118303395*

Janots, E., Engi, M., Berger, A., Allaz, J., Schwarz, J.-O. & Spandler, C. (2008), 'Prograde metamorphic sequence of REE minerals in pelitic rocks of the Central Alps: implications for allanite–monazite–xenotime phase relations from 250 to 610°C', *Journal of Metamorphic Geology* **26**(5), 509–526.
URL: *https://onlinelibrary.wiley.com/doi/abs/10.1111/j.1525-1314.2008.00774.x*

Jennings, E., Marschall, H., Hawkesworth, C. & Storey, C. (2011), 'Characterization of magma from inclusions in zircon: Apatite and biotite work well, feldspar less so', *Geology* **39**(9), 863–866.
URL: *https://doi.org/10.1130/G32037.1*

Jepson, G., Glorie, S., Konopelko, D., Gillespie, J., Danišík, M., Evans, N. J., Mamadjanov, Y. & Collins, A. S. (2018), 'Thermochronological insights into the structural contact between the Tian Shan and Pamirs, Tajikistan', *Terra Nova* **30**(2), 95–104.
URL: *https://onlinelibrary.wiley.com/doi/abs/10.1111/ter.12313*

Johnson, R. A. & Arca, M. S. (2010), 'Compilation Geologic Map from the Baboquivari Mountains to the Transition Zone of the Colorado Plateau'.

Jones, C. H., Lang Farmer, G., Sageman, B. & Zhong, S. (2011), 'Hydrodynamic mechanism for the Laramide orogeny', *Geosphere* **7**(1), 183–201.
URL: *https://doi.org/10.1130/GES00575.1*

Kellogg, K. S., Snee, L. W. & Unruh, D. M. (2003), 'The mesoproterozoic beaverhead impact structure and its tectonic setting, montana-idaho: 40ar/39ar and u-pb isotopic constraints', *The Journal of Geology* **111**(6), 639–652.
URL: *https://doi.org/10.1086/378339*

Kirkland, C., Yakymchuk, C., Gardiner, N., Szilas, K., Hollis, J., Olierook, H. & Steenfelt, A. (2020), 'Titanite petrochronology linked to phase equilibrium modelling constrains tectono-thermal events in the Akia Terrane, West Greenland', *Chemical Geology* **536**, 119467.
URL: *http://www.sciencedirect.com/science/article/pii/S0009254120300061*

Kohn, B. P. & Gleadow, A. J. W. (2019), Application of low-temperature thermochronology to craton evolution, *in* M. G. Malusà & P. G. Fitzgerald, eds, 'Fission-Track Thermochronology and its Application to Geology', Springer International Publishing, pp. 373–393.

Kusebauch, C., John, T., Whitehouse, M. J., Klemme, S. & Putnis, A. (2015), 'Distribution of halogens between fluid and apatite during fluid-mediated replacement processes', *Geochimica et Cosmochimica Acta* **170**, 225 – 246.
URL: *http://www.sciencedirect.com/science/article/pii/S0016703715005268*

Kylander-Clark, A. R., Hacker, B. R. & Cottle, J. M. (2013), 'Laser-ablation split-stream ICP petrochronology', *Chemical Geology* **345**, 99 – 112.
URL: *http://www.sciencedirect.com/science/article/pii/S0009254113000788*

Laslett, G. M., Kendall, W. S., Gleadow, A. J. W. & Duddy, I. R. (1982), 'Bias in measurement of fission-track length distributions', *Nuclear Tracks and Radiation Measurements* **6**(2), 79 – 85.
URL: *http://www.sciencedirect.com/science/article/pii/0735245X8290031X*

Lawton, T. F. (2008), Laramide Sedimentary Basins, *in* A. D. Miall, ed., 'The Sedimentary Basins of the United States and Canada', Vol. 5 of *Sedimentary Basins of the World*, Elsevier, pp. 429 – 450.
URL: *http://www.sciencedirect.com/science/article/pii/S1874599708000129*

Lister, G. S. & Davis, G. A. (1989), 'The origin of metamorphic core complexes and detachment faults formed during Tertiary continental extension in the northern Colorado River region, U.S.A.', *Journal of Structural Geology* **11**(1), 65 – 94.
URL: *http://www.sciencedirect.com/science/article/pii/0191814189900369*

Liu, L., Gurnis, M., Seton, M., Saleeby, J., Müller, D. R. & Jackson, J. M. (2010), 'The role of oceanic plateau subduction in the Laramide orogeny', *Nature Geoscience* **3**(5), 353–357.

Long, K. B., Gehrels, G. E. & Baldwin, S. L. (1995), 'Tectonothermal evolution of the Pinaleño-Jackson Mountain core complex, southeast Arizona', *GSA Bulletin* **107**(10), 1231–1240.
URL: *https://doi.org/10.1130/0016-7606(1995)107<1231:TEOTPO>2.3.CO;2*

Lu, Y. J., Loucks, R. R., Fiorentini, M., McCuaig, T. C., Evans, N. J., Yang, Z. M., Hou, Z. Q., Kirkland, C. L., Parra-Avila, L. A. & Kobussen, A. (2016), Zircon Compositions as a Pathfinder for Porphyry Cu ± Mo ± Au Deposits, *in* 'Tectonics and Metallogeny of the Tethyan Orogenic Belt', Society of Economic Geologists.
URL: *https://doi.org/10.5382/SP.19.13*

Mark, C., Cogné, N. & Chew, D. (2016), 'Tracking exhumation and drainage divide migration of the Western Alps: A test of the apatite U-Pb thermochronometer as a detrital provenance tool', *GSA Bulletin* **128**(9-10), 1439–1460.
URL: *https://doi.org/10.1130/B31351.1*

McDannell, K. T., Schneider, D. A., Zeitler, P. K., O'Sullivan, P. B. & Issler, D. R. (2019), 'Reconstructing deep-time histories from integrated thermochronology: An example from southern Baffin Island, Canada', *Terra Nova* **31**(3), 189–204.
URL: *https://onlinelibrary.wiley.com/doi/abs/10.1111/ter.12386*

McDowell, F. W., McIntosh, W. C. & Farley, K. A. (2005), 'A precise 40Ar–39Ar reference age for the Durango apatite (U–Th)/He and fission-track dating standard', *Chemical Geology* **214**(3), 249 – 263.
URL: *http://www.sciencedirect.com/science/article/pii/S0009254104004218*

Mueller, P. A., Burger, H. R., Wooden, J. L., Brady, J. B., Cheney, J. T., Harms, T. A., Heatherington, A. L. & Mogk, D. W. (2005), 'Paleoproterozoic Metamorphism in the Northern Wyoming Province: Implications for the Assembly of Laurentia', *The Journal of Geology* **113**(2), 169–179.
URL: *https://doi.org/10.1086/427667*

Mueller, P. A. & Frost, C. D. (2006), 'The Wyoming Province: a distinctive Archean craton in Laurentian North America', *Canadian Journal of Earth Sciences* **43**(10), 1391–1397.
URL: *https://doi.org/10.1139/e06-075*

Mueller, P. A., Heatherington, A. L., Kelly, D. M., Wooden, J. L. & Mogk, D. W. (2002), 'Paleoproterozoic crust within the Great Falls tectonic zone: Implications for the assembly of southern Laurentia', *Geology* **30**(2), 127–130.
URL: *https://doi.org/10.1130/0091-7613(2002)030<0127:PCWTGF>2.0.CO;2*

Nathwani, C. L., Loader, M. A., Wilkinson, J. J., Buret, Y., Sievwright, R. H. & Hollings, P. (2020), 'Multi-stage arc magma evolution recorded by apatite in volcanic rocks', *Geology* **48**(4), 323–327.
URL: *https://doi.org/10.1130/G46998.1*

Nishizawa, M., Takahata, N., Terada, K., Komiya, T., Ueno, Y. & Sano, Y. (2005), 'Rare-earth element, lead, carbon, and nitrogen geochemistry of apatite-bearing metasediments from the 3.8 ga isua supracrustal belt, west greenland', *International Geology Review* **47**(9), 952–970.
URL: *https://doi.org/10.2747/0020-6814.47.9.952*

Odlum, M. L. & Stockli, D. F. (2019), 'Thermotectonic evolution of the north pyrenean agly massif during early cretaceous hyperextension using multi-mineral u-pb thermochronometry', *Tectonics* **38**(5), 1509–1531.
URL: *https://agupubs.onlinelibrary.wiley.com/doi/abs/10.1029/2018TC005298*

Odlum, M. L. & Stockli, D. F. (2020), 'Geochronologic constraints on deformation and metasomatism along an exhumed mylonitic shear zone using apatite U-Pb, geochemistry, and microtextural analysis', *Earth and Planetary Science Letters* **538**, 116177.
URL: *http://www.sciencedirect.com/science/article/pii/S0012821X20301205*

Orme, D. A., Guenthner, W. R., Laskowski, A. K. & Reiners, P. W. (2016), 'Long-term tectonothermal history of laramide basement from zircon–he age-eu correlations', *Earth and Planetary Science Letters* **453**, 119 – 130.
URL: *http://www.sciencedirect.com/science/article/pii/S0012821X16304022*

O'Sullivan, G., Chew, D., Kenny, G., Henrichs, I. & Mulligan, D. (2020), 'The trace element composition of apatite and its application to detrital provenance studies', *Earth-Science Reviews* **201**, 103044.
URL: *http://www.sciencedirect.com/science/article/pii/S0012825219304180*

O'Sullivan, G. J., Chew, D. M., Morton, A. C., Mark, C. & Henrichs, I. A. (2018), 'An Integrated Apatite Geochronology and Geochemistry Tool for Sedimentary Provenance Analysis', *Geochemistry, Geophysics, Geosystems* **19**(4), 1309–1326.
URL: *https://agupubs.onlinelibrary.wiley.com/doi/abs/10.1002/2017GC007343*

Paton, C., Hellstrom, J., Paul, B., Woodhead, J. & Hergt, J. (2011), 'Iolite: Freeware for the visualisation and processing of mass spectrometric data', *Journal of Analytical Atomic Spectrometry* **26**(12), 2508–2518.

Peters, L., Ferguson, C. A., Spencer, J. E., Orr, T. R. & Dickinson, W. R. (2003), 'Sixteen $^{40}Ar/^{39}Ar$ geochronology analyses from southeastern Arizona', *Arizona Geological Survey Open File Report* p. 46.

Peyton, S. L., Reiners, P. W., Carrapa, B. & DeCelles, P. G. (2012), 'Low-temperature thermochronology of the northern Rocky Mountains, western U.S.A.', *American Journal of Science* **312**(2), 145–212.
URL: *http://www.ajsonline.org/content/312/2/145.abstract*

Pourmand, A., Dauphas, N. & Ireland, T. J. (2012), 'A novel extraction chromatography and MC-ICP-MS technique for rapid analysis of REE, Sc and Y: Revising CI-chondrite and Post-Archean Australian Shale (PAAS) abundances', *Chemical Geology* **291**, 38 – 54.
URL: *http://www.sciencedirect.com/science/article/pii/S0009254111003457*

976 Price, R. A. (1986), 'The southeastern canadian cordillera: Thrust faulting, tectonic wedging, and delam-
977 ination of the lithosphere', *Journal of Structural Geology* **8**(3), 239 – 254. International conference on
978 trusting and deformation.
979 **URL:** *http://www.sciencedirect.com/science/article/pii/0191814186900465*

980 Prowatke, S. & Klemme, S. (2006), 'Trace element partitioning between apatite and silicate melts',
981 *Geochimica et Cosmochimica Acta* **70**(17), 4513 – 4527.
982 **URL:** *http://www.sciencedirect.com/science/article/pii/S0016703706006120*

983 Reiners, P. W. & Brandon, M. T. (2006), 'Using thermochronology to understand orogenic erosion',
984 *Annual Review of Earth and Planetary Sciences* **34**(1), 419–466.
985 **URL:** *https://doi.org/10.1146/annurev.earth.34.031405.125202*

986 Rossel, P., Oliveros, V., Ducea, M. N., Charrier, R., Scaillet, S., Retamal, L. & Figueroa, O. (2013), 'The
987 Early Andean subduction system as an analog to island arcs: Evidence from across-arc geochemical
988 variations in northern Chile', *Lithos* **179**, 211 – 230.
989 **URL:** *http://www.sciencedirect.com/science/article/pii/S0024493713002776*

990 Rubatto, D. (2002), 'Zircon trace element geochemistry: partitioning with garnet and the link between
991 U–Pb ages and metamorphism', *Chemical Geology* **184**(1), 123 – 138.
992 **URL:** *http://www.sciencedirect.com/science/article/pii/S0009254101003552*

993 Rubatto, D. & Hermann, J. (2007), 'Experimental zircon/melt and zircon/garnet trace element partition-
994 ing and implications for the geochronology of crustal rocks', *Chemical Geology* **241**(1), 38 – 61. Crustal
995 Dynamics; links between geochronology and petrology.
996 **URL:** *http://www.sciencedirect.com/science/article/pii/S0009254107000782*

997 Saleeby, J. (2003), 'Segmentation of the Laramide Slab—evidence from the southern Sierra Nevada region',
998 *GSA Bulletin* **115**(6), 655–668.
999 **URL:** *https://doi.org/10.1130/0016-7606(2003)115<0655:SOTLSF>2.0.CO;2*

1000 Saylor, J. E., Rudolph, K. W., Sundell, K. E. & van Wijk, J. (2020), 'Laramide orogenesis driven by late
1001 cretaceous weakening of the north american lithosphere', *Journal of Geophysical Research: Solid Earth*
1002 **125**(8), e2020JB019570. e2020JB019570 2020JB019570.
1003 **URL:** *https://agupubs.onlinelibrary.wiley.com/doi/abs/10.1029/2020JB019570*

Schildgen, T. F., Hodges, K. V., Whipple, K. X., Reiners, P. W. & Pringle, M. S. (2007), 'Uplift of the western margin of the Andean plateau revealed from canyon incision history, southern Peru', *Geology* **35**(6), 523–526.
URL: *https://doi.org/10.1130/G23532A.1*

Schmidt, C. J. & Garihan, J. M. (1978), Laramide tectonic development of the rocky mountain foreland of southwestern Montana, *in* 'Rocky Mountain foreland basins and uplifts', Rocky Mountain Association of Geologists, pp. 271–294.

Schneider, S., Hammerschmidt, K., Rosenberg, C. L., Gerdes, A., Frei, D. & Bertrand, A. (2015), 'U–Pb ages of apatite in the western Tauern Window (Eastern Alps): Tracing the onset of collision-related exhumation in the European plate', *Earth and Planetary Science Letters* **418**, 53 – 65.
URL: *http://www.sciencedirect.com/science/article/pii/S0012821X15000989*

Schoene, B. & Bowring, S. A. (2006), 'U–Pb systematics of the McClure Mountain syenite: thermochronological constraints on the age of the $^{40}Ar/^{39}Ar$ standard MMhb', *Contributions to Mineralogy and Petrology* **151**(5), 615.
URL: *https://doi.org/10.1007/s00410-006-0077-4*

Schoene, B. & Bowring, S. A. (2007), 'Determining accurate temperature–time paths from U–Pb thermochronology: An example from the Kaapvaal craton, southern Africa', *Geochimica et Cosmochimica Acta* **71**(1), 165 – 185.
URL: *http://www.sciencedirect.com/science/article/pii/S0016703706020187*

Schudel, G., Lai, V., Gordon, K. & Weis, D. (2015), 'Trace element characterization of USGS reference materials by HR-ICP-MS and Q-ICP-MS', *Chemical Geology* **410**, 223 – 236.
URL: *http://www.sciencedirect.com/science/article/pii/S0009254115002934*

Seymour, N. M., Stockli, D. F., Beltrando, M. & Smye, A. J. (2016), 'Tracing the thermal evolution of the corsican lower crust during tethyan rifting', *Tectonics* **35**(10), 2439–2466.
URL: *https://agupubs.onlinelibrary.wiley.com/doi/abs/10.1002/2016TC004178*

Smith, M. E., Carroll, A. R., Jicha, B. R., Cassel, E. J. & Scott, J. J. (2014), 'Paleogeographic record of Eocene Farallon slab rollback beneath western North America', *Geology* **42**(12), 1039–1042.
URL: *https://doi.org/10.1130/G36025.1*

Smye, A., Marsh, J., Vermeesch, P., Garber, J. & Stockli, D. (2018), 'Applications and limitations of U-Pb thermochronology to middle and lower crustal thermal histories', *Chemical Geology* **494**, 1 – 18.
URL: *http://www.sciencedirect.com/science/article/pii/S0009254118303346*

Sonder, L. J. & Jones, C. H. (1999), 'Western united states extension: How the west was widened', *Annual Review of Earth and Planetary Sciences* **27**(1), 417–462.
URL: *https://doi.org/10.1146/annurev.earth.27.1.417*

Spear, F. S. & Pyle, J. M. (2002), 'Apatite, Monazite, and Xenotime in Metamorphic Rocks', *Reviews in Mineralogy and Geochemistry* **48**(1), 293–335.
URL: *https://doi.org/10.2138/rmg.2002.48.7*

Spencer, J. E. & Reynolds, S. J. (1990), 'Relationship between mesozoic and cenozoic tectonic features in west central arizona and adjacent southeastern california', *Journal of Geophysical Research: Solid Earth* **95**(B1), 539–555.
URL: *https://agupubs.onlinelibrary.wiley.com/doi/abs/10.1029/JB095iB01p00539*

Spencer, J. E., Richard, S. M., Lingrey, S. H., Johnson, B. J., Johnson, R. A. & Gehrels, G. E. (2019), 'Reconstruction of Mid-Cenozoic Extension in the Rincon Mountains Area, Southeastern Arizona, USA, and Geodynamic Implications', *Tectonics* **38**(7), 2338–2357.
URL: *https://agupubs.onlinelibrary.wiley.com/doi/abs/10.1029/2019TC005565*

Stacey, J. & Kramers, J. (1975), 'Approximation of terrestrial lead isotope evolution by a two-stage model', *Earth and Planetary Science Letters* **26**(2), 207 – 221.
URL: *http://www.sciencedirect.com/science/article/pii/0012821X75900886*

Stevens, A. L., Balgord, E. A. & Carrapa, B. (2016), 'Revised exhumation history of the Wind River Range, WY, and implications for Laramide tectonics', *Tectonics* **35**(5), 1121–1136.
URL: *https://agupubs.onlinelibrary.wiley.com/doi/abs/10.1002/2016TC004126*

Swan, M. M. (1976), 'The Stockton Pass fault: An element of the Texas lineament'.

Tagami, T. (1987), 'Determination of zeta calibration constant for fission track dating', *International Journal of Radiation Applications and Instrumentation. Part D. Nuclear Tracks and Radiation Measurements* **13**(2), 127 – 130.
URL: *http://www.sciencedirect.com/science/article/pii/1359018987900239*

1060 Tagami, T. & O'Sullivan, P. B. (2005), 'Fundamentals of Fission-Track Thermochronology', *Reviews in*
1061 *Mineralogy and Geochemistry* **58**(1), 19–47.
1062 **URL:** *https://doi.org/10.2138/rmg.2005.58.2*

1063 Terrien, J. J. (2012), The role of magmatism in the Catalina metamorphic core complex, Arizona: insights
1064 from integrated thermochronology, gravity and aeromagnetic data, PhD thesis, Syracuse University.

1065 Thomson, S. N., Gehrels, G., Joaquin, R. & Robert, B. (2012), 'Routine low-damage apatite U-Pb dating
1066 using laser ablation–multicollector–ICPMS', *Geochemistry, Geophysics, Geosystems* **13**(2).
1067 **URL:** *https://agupubs.onlinelibrary.wiley.com/doi/abs/10.1029/2011GC003928*

1068 Trail, D., Watson, E. B. & Tailby, N. D. (2012), 'Ce and Eu anomalies in zircon as proxies for the oxidation
1069 state of magmas', *Geochimica et Cosmochimica Acta* **97**, 70 – 87.
1070 **URL:** *http://www.sciencedirect.com/science/article/pii/S0016703712004905*

1071 Vermeesch, P. (2009), 'RadialPlotter: A Java application for fission track, luminescence and other radial
1072 plots', *Radiation Measurements* **44**(4), 409–410.

1073 Vermeesch, P. (2017), 'Statistics for LA-ICP-MS based fission track dating', *Chemical Geology* **456**, 19 –
1074 27.
1075 **URL:** *http://www.sciencedirect.com/science/article/pii/S0009254117301158*

1076 Vermeesch, P. (2018), 'Isoplotr: A free and open toolbox for geochronology', *Geoscience Frontiers*
1077 **9**(5), 1479 – 1493. SPECIAL ISSUE: Frontiers in geoscience:A tribute to Prof. Xuanxue Mo.
1078 **URL:** *http://www.sciencedirect.com/science/article/pii/S1674987118300835*

1079 Watson, E. & Cherniak, D. (2013), 'Simple equations for diffusion in response to heating', *Chemical*
1080 *Geology* **335**, 93 – 104.
1081 **URL:** *http://www.sciencedirect.com/science/article/pii/S0009254112005645*

1082 Weil, A. B. & Yonkee, W. A. (2012), 'Layer-parallel shortening across the Sevier fold-thrust belt and
1083 Laramide foreland of Wyoming: spatial and temporal evolution of a complex geodynamic system',
1084 *Earth and Planetary Science Letters* **357-358**, 405 – 420.
1085 **URL:** *http://www.sciencedirect.com/science/article/pii/S0012821X12005171*

1086 Wernicke, B. P., England, P. C., Sonder, L. J. & Christiansen, R. L. (1987), 'Tectonomagmatic evolution
1087 of cenozoic extension in the north american cordillera', *Geological Society, London, Special Publications*

28(1), 203–221.

URL: *https://sp.lyellcollection.org/content/28/1/203*

Whitmeyer, S. J. & Karlstrom, K. E. (2007), 'Tectonic model for the Proterozoic growth of North America', *Geosphere* **3**(4), 220–259.

URL: *https://doi.org/10.1130/GES00055.1*

Whitney, D. L., Teyssier, C., Rey, P. & Buck, W. R. (2013), 'Continental and oceanic core complexes', *GSA Bulletin* **125**(3-4), 273–298.

URL: *https://doi.org/10.1130/B30754.1*

Yonkee, W. A. & Weil, A. B. (2015), 'Tectonic evolution of the Sevier and Laramide belts within the North American Cordillera orogenic system', *Earth-Science Reviews* **150**, 531 – 593.

URL: *http://www.sciencedirect.com/science/article/pii/S0012825215300258*